UNIVERSITY OF GHANA

COLLEGE OF BASIC AND APPLIED SCIENCES

STRUCTURAL AND ALTERATION CONTROLS ON GOLD MINERALIZATION IN THE RHYACIAN ROCKS OF THE JOSEPHINE DEPOSIT, NW GHANA

BY

FUSEINI ATANGA

(10515036)

THIS THESIS IS SUBMITTED TO THE UNIVERSITY OF GHANA, LEGON IN PARTIAL FULFILMENT OF THE REQUIREMENT FOR THE AWARD OF MPHIL IN GEOLOGY DEGREE.

DEPARTMENT OF EARTH SCIENCE

JULY, 2022.

DECLARATION

I, Fuseini Atanga, declare that this thesis is my work produced from research under supervision towards the award of MPHIL in Geology degree in the Department of Earth Science, University of Ghana. It contains no material previously published by another person or accepted for the award of any other degree of the university or any other university, except where due acknowledgment has been made in the text.

..... Date 13/09/2022

Fuseini Atanga

(MPhil. Candidate)

..... Date 13/09/2022

Dr. Prince Ofori Amponsah

(Principal Supervisor)

..... Date 13:09:2022

Prof. Prosper Mackenzie Nude

(Co. Supervisor)

ABSTRACT

This thesis focuses on the structures and alterations controlling gold mineralization in the Josephine deposit found in NW Ghana. The lithological and structural maps were produced from field lithological and structural data in conjunction with airborne geophysical data. The lithologies observed in the deposit comprise of meta-sediments (mainly quartzite), granitoid batholiths, mafic intrusion (dolerite), and gneiss. The quartzite which hosts the mineralization have experienced greenschist metamorphism. Through mapping and structural analysis, the following sequence of deformational events; D_{JO0}, D_{JO1}, D_{JO2} and D_{JO3} was identified. D_{JO0} is synonymous to the primary preserved sedimentary features observed in the rocks and mainly observed in the quarzitic rocks.

Gold mineralization in the deposit is structurally controlled and mainly associated with the D_{JO1} NNW-trending dextral and steeply dipping sinusoidal shear zone. The gold occurs together with arsenopyrite along the foliation planes of the host rocks, quartzite. Alteration minerals assemblage observed within the deposit give indication the gold precipitated under greenschist metamorphic facies.

The ore body geometry is about 15-40m wide with a strike length of 800m trending in the NNW direction. Silicification, seritization, chloritization and sulphidation (quartz + sericite + chlorite + sulphide) are the main alterations associated with the ore zone in the deposit.

Sulphides observed in the deposit are arsenopyrite, pyrite, chalcopyrite and sphalerites with gold more associated with the arsenopyrite mineral. The gold occurs as free gold within the fractures of the arsenopyrite mineral. The pathfinder elements associated with gold in the deposits are mainly antimony or stibnite (Sb), Te (Tellurium), S (Sulphur), Cu (Copper), Ag (Silver), and Lead (Pb) which is characteristic of orogenic gold. Isocon analysis suggests the altered mineralized zone has gained 16.6% mass and volume increase because of addition of the fluids. This together with the

zonation of the arsenopyrite gives an indication of hydrothermal process responsible for the mineralization with an unknown source.

DEDICATION

This thesis is dedicated to Allah, my family, and my friends.

ACKNOWLEDGMENT

I am grateful to the Tullow Ghana scholarship scheme and Agate project for the funding granted me throughout this M.Phil. work. Special thanks go to Azumah resources Limited for granting me the permission to use the Josephine deposit for this thesis work and the accommodation and means of transportation given to me during the fieldwork.

My profound gratitude goes to Dr. Prince Ofori Amponsah for the confidence he had in me by taking me as his student, proposing this project, and the sacrifices he made in guiding me throughout this project work. I say a big thank you to Prof. Prosper Mackenzie Nude for also accepting to be a part of this project and for the wise advice and guidance he gave me.

I would like to thank Prof. Thomas Mba Akabzaa, Prof. Patrick Asamoah Sakyi, Dr. Samuel Nunoo, and Dr. Daniel Kwayisi for their help and expert contribution in terms of the geology of the deposit and other aspects of this work. I also wish to thank my friend, Kojo Selete Avemegah for his support during this work.

Last but not least, I would like to thank my family; my parents, and my siblings for their support, prayers, and patience during this work.

TABLE OF CONTENTS

DECLARATION I
ABSTRACT II
DEDICATION IV
ACKNOWLEDGMENT V
CHAPTER ONE 1
INTRODUCTION 1
1.1 Background and Justification 1
1.2 Structure of the thesis 4
1.3 Geography 4
CHAPTER TWO 8
LITERATURE REVIEW 8
2.1 Regional Geology 8
2.2 The geology of the study area 13
2.3 The Structural and Metamorphic Architecture of NW Ghana 14
2.4 Gold deposits in the Paleoproterozoic Birimian in Ghana 16
CHAPTER THREE 19
MATERIALS AND ANALYTICAL METHODS 19
3.1 Desk Study 19
3.2 Field work 19
3.3 Laboratory work 21
CHAPTER FOUR 26
RESULTS 26
4.1 Lithological description and metamorphic mineral assemblages 26
4.1.1 Lithological description 26
4.2 Structural features and Deformation 41
4.2.1 D_{JO0} Deformational Regime 43
4.2.2 D_{JO1} Deformational Regime 44
4.2.3 D_{JO2} Deformational Regime 45
4.2.4 D_{JO3} Deformational Regime 46
4.3 Alteration 48
4.4 Ore body characteristics and geometry 50
4.5 Isocon Analysis (Mass-Balance considerations) 51

4.5 Ore Mineralogy 56
CHAPTER FIVE 58
DISCUSSION 58
5.1 structural and alteration controls on gold mineralization in the Josephine deposit 63
5.1.1 Structural controls on mineralization 63
5.1.2 Alteration controls on mineralization 64
CHAPTER SIX 66
CONCLUSION 66
RECOMMENDATION 67
REFERENCES 68
Appendix 1: Attitude of Bedding plane 77
Appendix 2: Attitude of foliation (S_{JO1}) 78
Appendix 3: Attitude of foliation (S_{JO2}) 79
Appendix 4: Attitude of foliation (S_{JO3}) 80
Appendix 5: Attitude of lineation (L_{JO1}) 81
Appendix 6: Attitude of lineation (L_{JO2}) 82

LIST OF FIGURES

Figure 1. A Map of the northern part of Ghana showing Azumah permits which includes the Josephine PL (the red rectangular box;Fig. 1a), and their location on the insert Ghana map (Fig. 1b) (after Azumah resource limited, 2015)……...3

Figure 2. Geopolitical map of Ghana showing major towns in the country (Mapsland, 2021). The green rectangular box shows the study area……..5

Figure 3. A picture showing the vegetation of the study area in the dry season……...7

Figure 4. Simplified map of Africa and simplified geological map of the Leo-Man shield. Also shown is an insert of the map of Africa showing the location of the Birimian domain of the West African Craton (modified after Milési et al., 2004)…….9

Figure 5. Simplified geological map of Ghana showing the structural architecture of the greenstone belts and intervening basins (Castle Mineral Resources, 2013)……10

Figure 6. A Map of part of the Leo-Man shield of the West African craton showing the distribution of gold deposits and mines (modified after Milési et al., 2004). Insert in red is the Josephine deposit, a part of the Wa-Gold project owned by Azumah Resources limited which is the focus of this MPhil research…….....17

Figure 7. Outcrop map showing the distribution of the various rock types in the study area……..27

Figure 8. Field photographs illustrating the outcrops encountered in the study area (a) granodiorite (b) granite showing shearing (c) diorite with mafic xenoliths and (d) veining in diorite……31

Figure 9. Photomicrographs showing (a) hypidiomorphic-granular texture, (c and d) pyrite and idiomorphic hornblende: Note the association between biotite and arsenopyrite (d). Qz=quartz, Bt=biotite, Kfs=k-feldspar, Apy= arsenopyrite, Py=pyrite, Chl=chlorite, Hbl=hornblende, ms=microcline Ser=sericite. pl=plagioclase……..32

Figure 10. Field photograph of quarzitic rocks showing (a) tabular cross stratification in quartzite (b) mineral stretching lineation in quartzite (c) folding in quarzitic schist and (d) boudinage quartz vein quarzitic schist……34

Figure 11. Photomicrographs of quartzite showing porphyroblastic texture (a), granilitic texture (b) and schistose texture (c to f): Note the association between biotite and the sulphides. Qz=quartz, Bt=biotite Chl=chlorite, Py=pyrite, Po=pyrrhotite Kfs=K-feldspar……...35

Figure 12. Field photographs showing dolerite sill intrusion in granitoid (a) quartzo-feldspathic veins (b)……..36

Figure 13. Photomicrographs showing shearing in dolerite (a) mineral elongation (b), and clino-and-ortho-pyroxene as well as sub-ophitic texture (c). Qz=quartz, Pl=plagioclase, Amp=amphibole, Px= pyroxene Cpx=Clinopyroxene, Opx=Orthopyroxene Chl=chlorite, Bt=biotite Opq=opaque mineral…….38

Figure 14. (a) Field photograph of gneiss showing gneissic banding, (b) photomicrograph of the mineral assemblage within the gneissic rock in the study area, (c) perthitic texture in porphyroblast k-feldspar and quartz showing undulose extinction (d) k-feldspar porphyroblast with inclusions and stretched quartz Qz=quartz, Pl=plagioclase, Amp=amphibole, Kfs=K-feldspar, Bt=biotite……...40

Figure 15. A simplified Structural map of the study Josephine deposit compiled from field measurements and structural fabric interpreted from geophysical data. Inserts are lower hemisphere stereographic projection for poles of the different deformational generation of foliation and lineaments……42

Figure 16. Field photograph illustrating (a) preserved sedimentary layering (cross bedding) and (b) an inserted Schmidt plot showing the general trend of the beds……43

Figure 17. Field photographs showing (a, b) S_{JO1} foliation and boudins indicating the top-to-the-NE kinematic indicator and dextral sense of movement (c) F_{JO1} isoclinal folds defining the S_{JO1} foliation and (d) an inserted Schmidt plot showing the general dip and trend of the S_{JO1} foliation. ……45

Figure 18. Field photographs illustrating (a) S_{JO2} and S_{JO3} foliation defined by F_{JO2} open fold and F_{JO3} folds respectively and (c, d) their respective inserted Schmidt plot showing the general dips and trend of the foliations……...46

Figure 19. Field photographs illustrating dextral faulting associated with the final stage of deformation, D_{JO3}……...47

Figure 20. Field photographs illustrating (a, b) ptygmatic folding interpreted to represent the third generation of folding associated with D_{JO3} deformation, (c) inserted Schmidt plots illustrating their dip and trend of S_{JO3} foliation and (d) E-W space cleavages formed as a result of E-W directed horizontal contraction observed in the granitoid……48

Figure 21. Photomicrograph showing the alteration mineral assemblage in the ore zone (a) shows the alteration mineral assemblage of quartz, chlorite and arsenopyrite with minor biotite (b) shows alteration mineral assemblage of quartz, sericite and arsenopyrite with minor micas. Qz=quartz, Ser=Sericite, Pl=plagioclase, Ch=chlorite, Bt=biotite Apy=Arsenopyrite, Ms=muscovite……...49

Figure 22. Cross-section (looking east) of the Josephine deposit along 576,450 mE showing the main ore body, along the NNW dextral D_{JO1} shear dipping 70-80° NE. High-grade mineralization is restricted to 15m to 40m thick alteration zone with alteration mineral assemblage of quartz+chlorite+sericite+sulphides……50

Figure 23. Isocon diagrams constructed (using the EASYGRESGRANT MS-Excel sheet in Lopez-Moro (2012); based on the theoretical development by Gresens', 1967 and built upon by Grant (1986)) for five pairs each of unaltered and altered quartzites from the main ore zone. (a) the Isocon diagram (b) shows a close-up of the red insert in (a)……...53

Figure 24. SEM images of arsenopyrites in the Josephine deposit (a) disseminated Arsenopyrite (b) gold occurrence in arsenopyrite (c) growth of chalcopyrite on arsenopyrite and (d) irregular sector zoning in arsenopyrite. Au=gold, Cu=copper, Apy=Arsenopyrite, Ccp=chalcopyrite…...57

Figure 25. A simplified composite map of the Josephine deposit compiled from field data and geophysical data interpretation showing the lithological units, artisanal pits, and structures from both field measurement and geophysical data……59

LIST OF TABLES

Table 1: Mineralogical composition of granitoid using visual estimation charts after Terry and Chilingar (1995)…….28

Table 2. Major and trace element analytical data of the mineralized quartzites in the Josephine deposit……52

Table 3. Whole-rock geochemical data from the alteration zone in the quartzites used for the isocon calculations……54

Table 4. Table comparing the structures observed within the Josephine deposit and that of the regional deformation sequence proposed by Block (2015) and Baratoux et al., (2011)……62

CHAPTER ONE

INTRODUCTION

1.1 Background and Justification

Ghana is among the leading producer of gold in Africa (International trade organization, 2020). Gold production is critical to the economy of Ghana. It accounts for approximately 95% of the country's minerals revenue and provide significant employment to the people.

Studies of gold deposits in the Birimian of Ghana, especially the southern parts of the country started in the late 1800s to early 1900s focusing mainly on their genetic type and prospectivity (Allibone et al., 2002; Feybesse et al., 2006; Fougerouse et al., 2017; Oberthür et al., 1998; Perrouty et al., 2012). However, exploration in the Birimian of NW Ghana which is dated to be of Rhyacian age (2300 to 2050 MA) only started in the 1960s by the Russian technical team (Griffis et al., 2002). It is therefore not surprising that the Birimian in NW Ghana is generally less studied as compared to that in the South.

The continued increase in gold prices, averaging about 9.67% from 2000 to 2021 (Macrotrends, 2021), and the relevance of gold to the economy of Ghana, has provided the impetus for both industry and academia to focus its efforts on finding and understanding the occurrence of this valuable mineral. These reasons necessitated the beginning of this research project in the Josephine deposit, NW Ghana

This thesis is designed to study the Josephine deposit part of the Azumah Resources Wa Gold Project of gold inventory in Northwest Ghana (Fig. 1a). Azumah Resources Limited (now Ibaera Capital) has been exploring NW Ghana for gold since 2006 (Fig.1b). So far, exploration activity

in this area has resulted in approximately 2.8 million ounces (Moz) of gold, with 1.37 Moz of measured and indicated gold, and 1.63 Moz of inferred gold at an average grade of 1.92 gram per tonne g/t (Ibaera Capital, 2021). Most of the geological settings hosting the precious metal on Azumah Resources Limited tenements (Fig. 1b) have been thoroughly studied through the works of (Amponsah et al., 2016; Amponsah et al., 2015; Salvi et al., 2016), however, the structural setting and alteration control on gold mineralization on the Josephine deposit is not fully understood.

The overarching objective of this thesis is to study and resolve the structural and alteration controls of the Rhyacian rocks hosting the gold mineralization in the Josephine deposit and to answer the following specific questions;

1. What is the relative timing between deformation and gold mineralization?
2. How does the hydrothermal plumbing system affect the alteration associated with the mineralization?

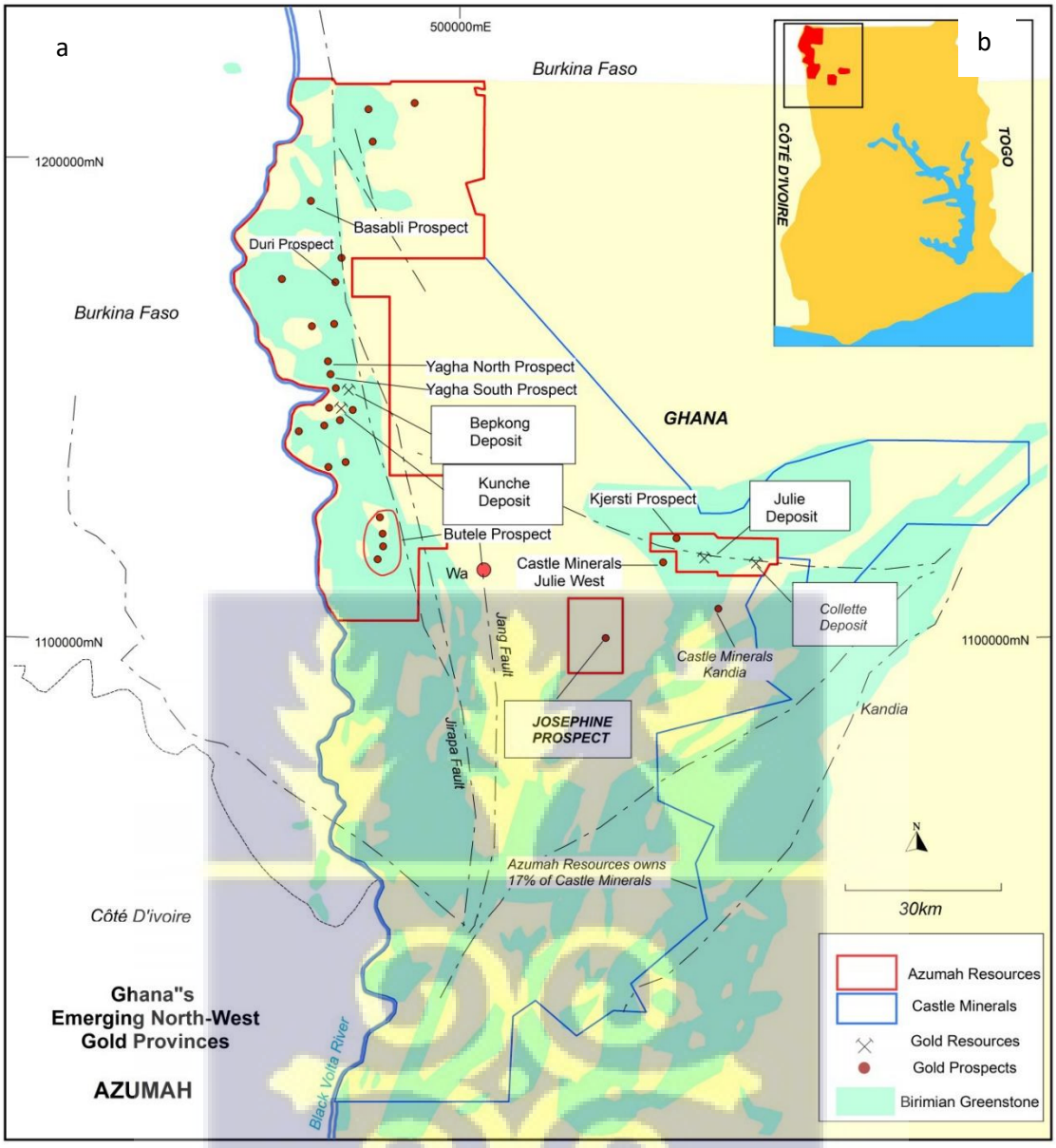

Figure 1. A Map of the northern part of Ghana showing Azumah permits which includes the Josephine PL (the red rectangular box;Fig. 1a), and their location on the insert Ghana map (Fig. 1b) (after Azumah resource limited, 2015)

1.2 Structure of the thesis

The thesis is organised in six chapters. The first three chapters will concentrate on the general introduction (chapter 1), chapter 2 reviews the literature pertaining to this research and chapter 3 describes the methodology used for the research. The next chapter will focus on the results obtained from the field work and laboratory analysis (chapter 4). The results will then be interpreted and discussed in chapter 5 and conclusion drawn in chapter 6.

1.3 Geography

1.3.1 Study Area and accessibility

The study area (Josephine PL; Fig. 1a; Fig. 2) is located in the Wa East district of the Upper West Region of Ghana. The Josephine PL lies within the coordinates, (569500 mN, 1109100 mE), (579500 mN, 119100 mE), (569500 mN, 1094500 mE) and (579500 mN, 1094500 mE) using UTM, zone 30 of the WGS 84 ellipsoid. The study area is situated ~ 26 km southeast of Wa (the regional capital) and covers a total area of 141.9 km^2. There is a 2 km airstrip in Wa as well as a very good network of roads connecting major towns and villages in the study area. This makes the study area readily accessible.

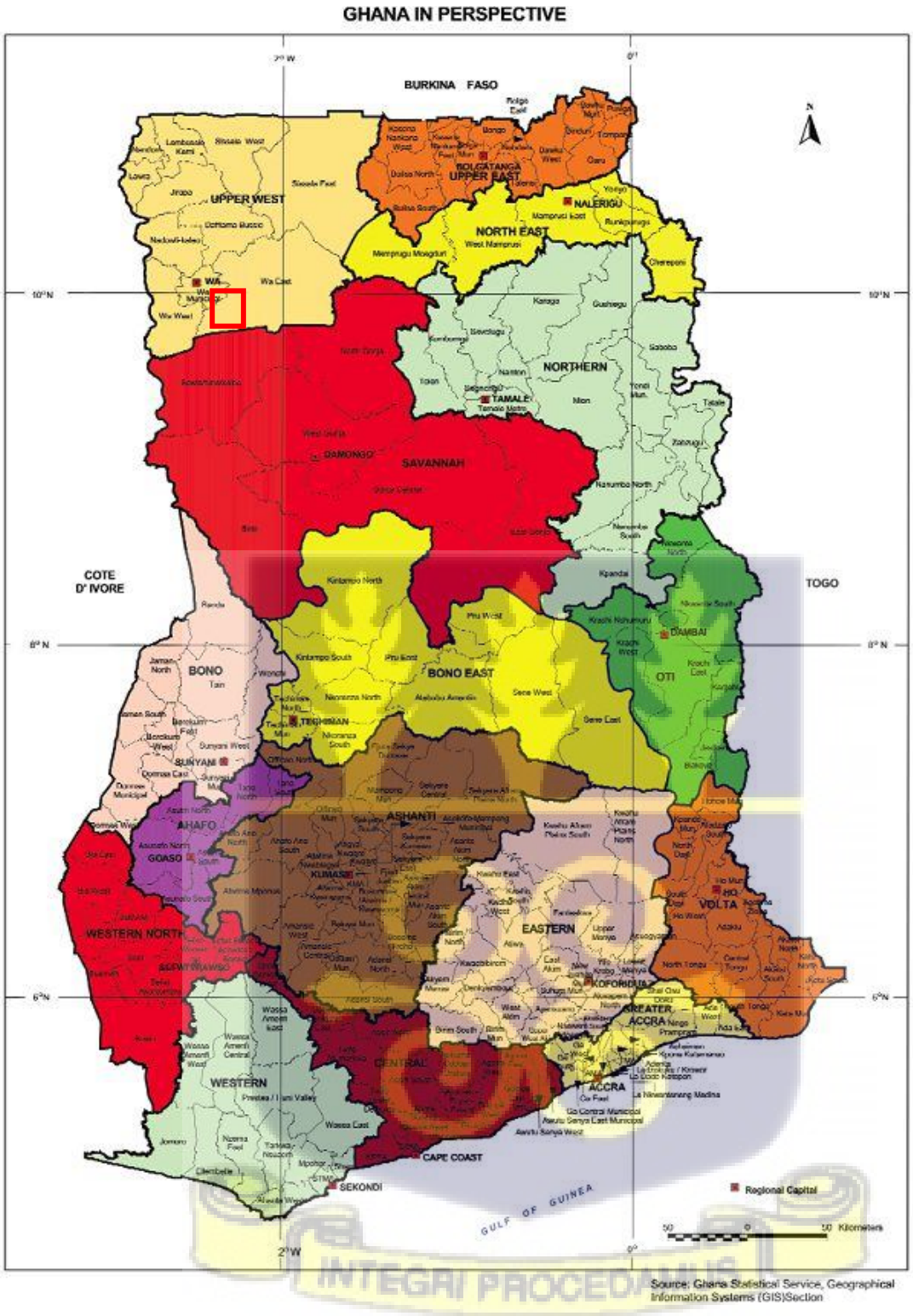

Figure 2. Geopolitical map of Ghana showing major towns in the country (Ghana statistical service, 2019). The red rectangular box shows the study area.

1.3.2 Relief and Drainage

Apart from a few scattered hills that trend in the N-S direction with heights between 350 to 450 m, most of the study area is generally flat as a result of intense erosion. Drainage in the study area is ensured by the Black-Volta River located to the west of the area. The black Volta also forms a border between Ghana and Burkina Faso. According to (Petr, 1986), The Black Volta is fed by numerous tributaries, including the Bepkong, Kulpawn, and Felin. ((Dickson & Benneh, 1988; Jin et al., 2018; McCartney et al., 2012)

1.3.3 Climate, Soils and Vegetation

The study area is in the Guinea savannah vegetation zone, which is distinguished by tall grasses interspersed with fire-resistant, smaller deciduous trees (Government of Ghana, 2020b) (Fig. 3). According to Dickson and Benneh (1988) and the (Government of Ghana, 2020a), the primary soil in the area is laterite, which is formed from the Birimian rocks. The Ghana Meteorological Agency (GMA), in 2020 reported that the study area's climate is tropical, with a lengthy dry-season lasting from October -to- April, with February and April being the warmest months. The climate here is classified as Aw by the Köppen-Geiger system. The area has one rainy season annually with about 1033mm mean annual rainfall. Its starts in May, peaks in between June and July and ends around late September to early October. The average annual temperature and relative humidity are 28.1 °C and 61 % respectively.

Figure 3. A picture showing the vegetation of the study area in the dry season.

CHAPTER TWO

LITERATURE REVIEW

In this chapter, general insight is given on the 2.2Ga to 2.1Ga tectono-metamorphic Bimimian domain in Ghana. Also elucidated is its relationship with other domains in the West African craton (WAC), the sedimentary basins associated with it, and its structural evolution.

Finally, some insight is given on the geology of the study area as well as gold mineralization in Ghana explaining its occurrence, the rock types they are associated with, mineral paragenesis, and associated sulphides.

2.1 Regional Geology

2.1.1 Summary of the Birimian in Ghana

The Birimian domain in Ghana, is part of the Paleoproterozoic portion of the West-African Craton's Leo-Man Shield (WAC) (Abouchami et al., 1990; Boher et al., 1992; Feybesse et al., 2006; Hirdes et al., 1992; Taylor et al., 1994; Vidal et al., 2009). The X-shaped Birimian domain of West Africa is composed of an eastern Paleoproterozoic section called the Leo-Man Shield, with an Archean age Kenema-Man section juxtaposed to the western part of the Leo-Man Shield (Fig.4). The WAC straddles the western half of Ghana, Eastern half of the Ivory Coast, Senegal and Mauritania and northwards form Burkina Faso to Mali and Niger.

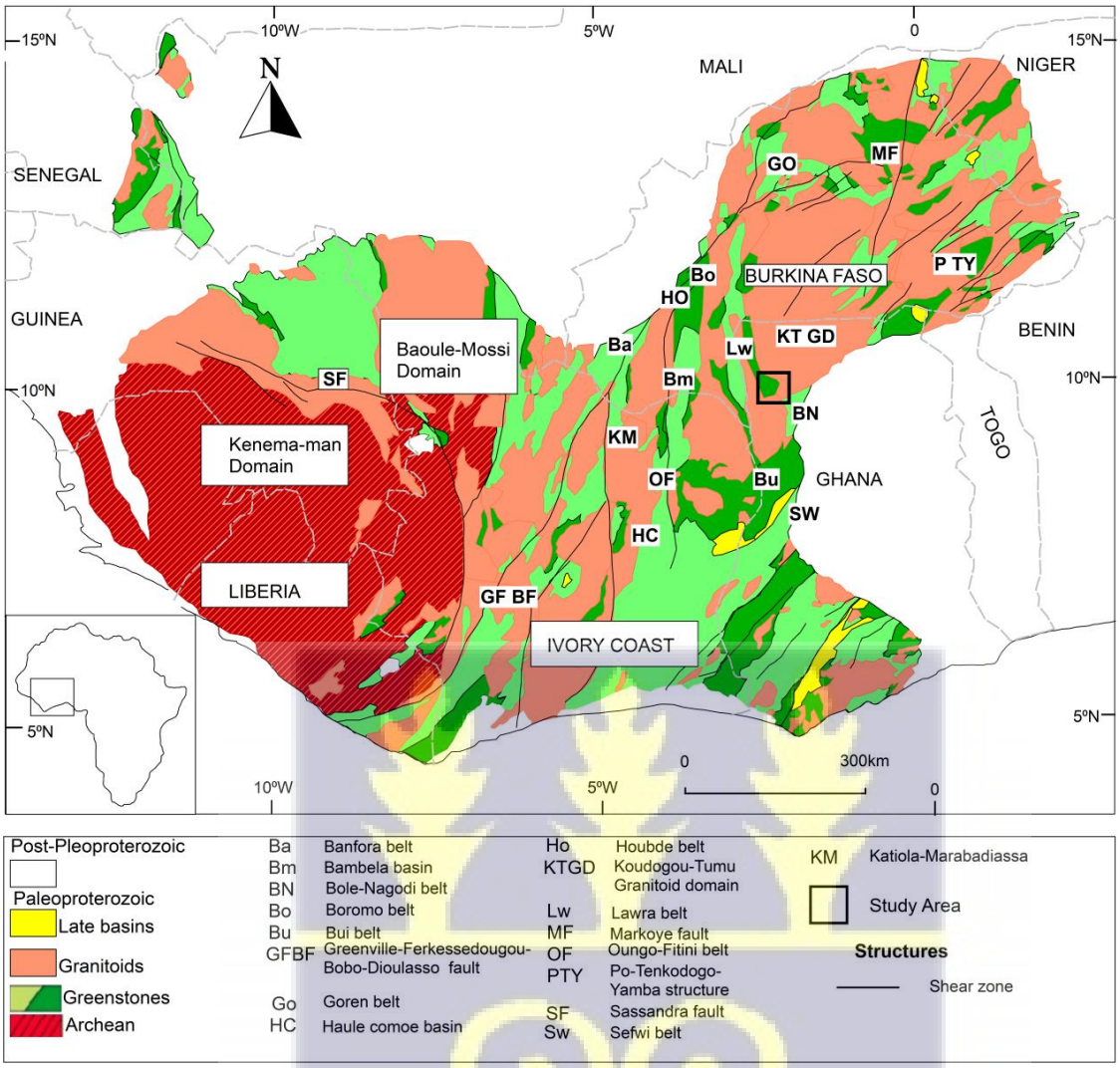

Figure 4. Simplified map of Africa and simplified geological map of the Leo-Man shield. Also shown is an insert of the map of Africa showing the location of the Birimian domain of the West African Craton (modified after Milési et al., 2004).

The Birimian is distinguished by an extended metavolcanic greenstone belt (Fig. 5), metasedimentary basins, and granitoid units composed of variably deformed grey gneiss and tonalite-trondhjemite-granodiorite (TTG) usually distinguished by craton-scale shear zones (e.g., the Sassandra shear zone (Abouchami et al., 1990; Feybesse & Milési, 1994). Kitson (1918) reported the first volcanic and volcano-sedimentary units for the Birimian Supergroup in Ghana's Birim Valley. The greenstone belts are composed mostly of metamorphosed bi-modal volcanic

sequences of calc-alkaline and tholeiitic basalts, rhyolites mostly associated with minor chemical sedimentary (i.e.; cherts, gondites and jasper) units and volcaniclastic (Baratoux et al., 2011; Boher et al., 1992; Doumbia et al., 1998; Pouclet et al., 2006). The Birimian volcano-sedimentary units are composed of low-grade metamorphic, greywacke, shale, chert, argillite and intercalated intermediate volcanoclastic or volcanic strata (Adadey et al., 2009; Duodu, 2009; Junner, 1940).

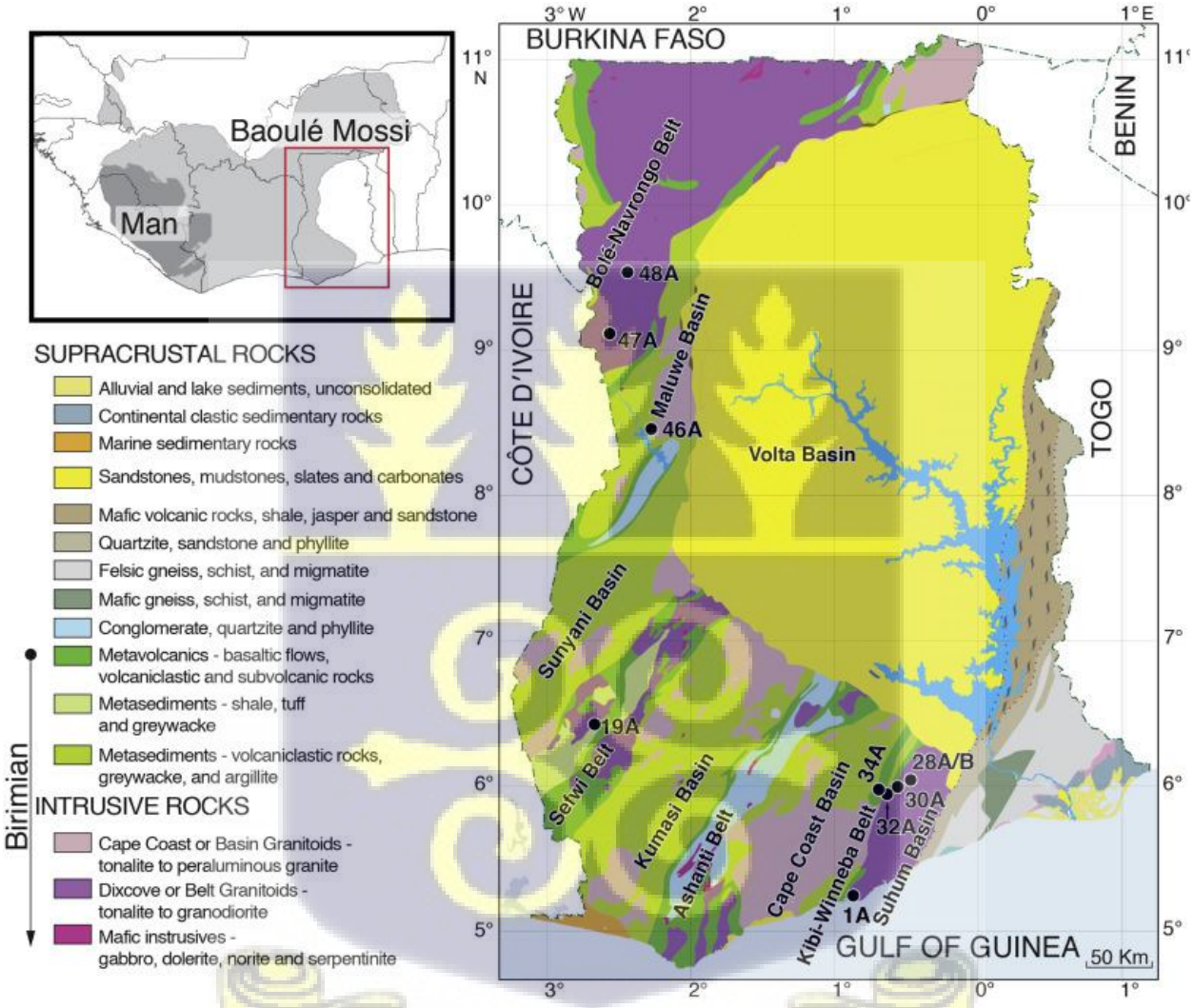

Figure 5. Simplified geological map of Ghana showing the structural architecture of the greenstone belts and intervening basins (Petersson et al., 2018)

2.1.2 The Tarkwaian Sedimentary rocks

The Tarkwaian was first identified by Kitson (1918) and Whitelaw and Junner (1929). It represents fluvio-deltaic detrital sedimentary formations which are generally confined to fault constrained basins overlaying core sections of greenstone belts in the earliest Paleoproterozoic sequence (Ledru et al., 1994). Tarkwaian rock units are composed of conglomerates, quartzites, and immature sediments that are characterized by the sequences revealed in southern Ghana's Ashanti Belt (Junner & Wild, 1935; Perrouty et al., 2012). The Kawere group, composed of metamorphosed sandstone and conglomerate make up the base of the sedimentary sequence. This is followed by the gold bearing Banket series which is made up of interbedded layers of metamorphosed sandstones and conglomerate. The thick Tarkwa phyllites overlay the Banket series and on the very top of these units is the Huni sandstone. The timing of deposition by detrital zircons (single U-Pb and Pb-Pb dating) from the formation's basal units, yielded ages ranging between ca. 2150 and 2143 Ma (Davis et al., 1994). The maximum age of deposition was then updated to 2107 – 2097 Ma (Perrouty et al., 2012; Pigois et al., 2003). The sediments in the Tarkwa Group are interpreted as syn-orogenic to late-stage basins (Davis et al., 1994; Perrouty et al., 2012), or as a molasses series deposited at the start of deformation in a foreland basin (Davis et al., 1994; Eisenlohr & Hirdes, 1992).

2.1.3 Tectonic Evolution and Eburnean Orogeny

Many researchers have described the structural evolution of the Birimian domain as polycyclic events (Eisenlohr & Hirdes, 1992; Feybesse et al., 2006; Ledru et al., 1994; Milési et al., 1992). Ledru et al. (1988), Milési et al. (1992), and Perrouty et al. (2012) proposed two major phases of deformation: Pre-Tarkwaian (D_1) and Post Tarkwaian (D_2). Eisenlohr and Hirdes (1992)identified two stages or intensities of deformation. Thus, a low strain and high strain deformation phases.

The rocks formed NE subvertical foliation during the low strain phase (S_1) and sub-parallel to bedding with a sub-horizontal intersection L_1 lineation. High strain phase rocks are found primarily along the NW edges of volcanic belts and are distinguished by the availability of a penetrative northeast trending foliation (S_2) and a SW plunging stretching lineation.

Feybesse et al. (2006) identified three main phases of deformation within Ghana's Birimian domain. D_1 deformation is characterized by an initial S_1 foliation which is parallel to the axial plane of microfolds. The penetrative fabrics formed during this stage differ depending on the degree of metamorphism and the degree of co-axial strain associated with the deformation. Non-transposition of beds, stretching lineation and symmetrical pressure shadows are all products of the coaxial deformation. The D_2 deformation phase results from the maximum strain, and is manifested by F_2 folds with horizontal or slightly plunging hinges, linked with a general E-NE to W-SW striking S_2 cleavages and NE to SW sinistral ductile faults with reverse components. Folds associated with brittle shears define D_3 deformational event, indicating that the crust has already been exhumed to higher structural levels.

The Eburnean in Ghana was proposed by Feybesse et al. (2006) to have an early phase between 2135Ma and 2100Ma which corresponds to magmatic accretion and plutonism that ended with the formation of the Sunyani and Kumasi-Afema Basin. The Eburnean orogeny Ca. 2130– Ca.1980Ma correlates to thrust tectonism defined by sinistral transcurrent deformation in the Ashanti Belt. Allibone et al. (2004) postulated two-phase Eburnean evolution, which divided into the Eburnean I (2200–2150Ma) and Eburnean II (2116–2088Ma). In northern Ghana, De Kock et al. (2011) also observed two phases of the Eburnean event, which he termed as Eoe-Eburnean (2160 to 2150 Ma) and Eburnean (2148 to 2090 Ma), respectively. Eoe-Eburnean began with the rifting of the Bole-Navrongo crust between 2148 to 2125Ma which led to the development of the Maluwe basin

and followed by younger magmatic episodes between 2122Ma to 2118Ma. Crustal thickening from 2114Ma to 2090Ma resulted into the hydrothermal alteration and the epidote-amphibolite-grade metamorphism. Generally, De Kock et al. (2011) Eoeburnean and Eburnean defined in northern Ghana correlates with what has been defined in the south by Allibone et al. (2002).

Allibone et al. (2002) suggests that the Eburnean I event resulted from a period of magmatism and metamorphism responsible for the Sefwi Group metavolcanics and TTG granitoid emplacement that correlates with the pre-Eburnean of Feybesse et al. (2006).

2.2 The geology of the study area

The geology of NW Ghana as described by Block et al. (2016), can be divided into five domains: the Wa-Lawra belt, the Bole-Bulenga domain, the Koudougou-Tumu domain, the Bole-Nangodi belt, and the Julie belt.

The Wa-Lawra belt in northern Ghana, represents the southern extension of the larger Boromo belt (Amponsah et al., 2015), and is fault-bounded to the east by the Koudougou-Tumu domain. This fault is known as the Jang fault. The Jirapa shear zone, a crustal scale transcurrent (greater than 200 km) shear zone formed during the Paleoproterozoic period and divides the Wa-Lawra belt into two halves (eastern and western parts). The eastern part is made up of regionally metamorphosed and deformed 2139 ±2 Ma sediments such as greywackes, volcano-sedeiments, shales, greywacke, and volcanic rocks (Amponsah et al., 2015; Block et al., 2015) and early syntectonic 2212± 1 Ma to 2153 ± 4 Ma; (Duodu, 2009; Sakyi et al., 2014) granitoids. Intruding these rocks are the late 2104 ± 4 Ma granitoids, which appear to be undeformed. The western portion is made up of high grade gneisses and granitoids from 2187 ±3 Ma (Duodu, 2009; Sakyi et al., 2014) The rocks have been affected by amphibolite facies metamorphism.

The Koudougou-Tumu domain is made up of 2162± 1 Ma to 2134 Ma gneisses and gabbro intruded by 2128 late porphyritic granites (Amponsah et al., 2015; Duodu, 2009)

The Julie belt and the Bole-Bulenga domain are located south of the Koudougou-Tumu domain. The Julie belt is made up of basalts, volcano-sedimentary rocks, and TTGs with granodioritic affinities that have all been metamorphosed to the greenschist facies (Amponsah et al., 2015; Block et al., 2015) determined an age of 2129 ± 7 Ma in the volcaniclastics.

The Bole-Bulenga domain is made up of high grade paragniesses intruded by orthogneisses with crystallization ages ranging from 2195 Ma to 2135 Ma. The Bole-Nangodi shear zone is located to the south of the Bole-Bulenga domain and the Julie belt. Their boundary is defined by NE-SW crustal scale shear zones (Block et al., 2015). The belt is made up of shales, volcaniclastic rocks, granites, and gneisses with crystallization ages ranging from 2196 1 Ma to 2118 3 Ma (De Kock et al., 2011; Duodu, 2009).

The Bole-Bulenga domain is made up of high-grade paragneisses intruded by orthogneisses with ages of crystallization ranging from 2195 to 2135 Ma. To the south, the Bole-Bulenga domain and the Julie belt border the Bole-Nangodi shear zone. Shear zones on the crustal scale run NE-SW along the boundary (Block et al., 2015). The belt is made up of shales, volcaniclastics, granites, and gneisses with crystallization ages ranging from 2196 ±1 Ma to 2118 ±3 Ma (De Kock et al., 2011; Duodu, 2009).

2.3 The Structural and Metamorphic Architecture of NW Ghana

The initial deformation, D_1 in NW Ghana is defined by thrust faults forming E-W S_1 foliation fabrics and L_1 stretching lineation. The basalts, volcano-sedimentary rocks and TTG in the Julie belt terrane were all affected by this deformation. According to Block et al. (2015), the regional

foliation is marked by mineral assemblages typical of regional metamorphism and occurred around 2139 to 2123 Ma. D_1 is mostly characterized by greenschist facies metamorphism believed to have been retrograded from amphibolite facies metamorphic event in NW Ghana (Block et al., 2015).

P-T conditions shows that the metamorphic overprint defined by regional amphibolite facies do not exceed 11 kbars and the temperatures do not exceed 600°C, whilst that of the greenschist facies retrogressed between 230°C and 350°C and pressures ranging from 1 to 3 kbar. Peak metamorphism occurs between 2144 and 2123 Ma (Block et al., 2015).

The mineral assemblages that characterise the greenschist facies comprises muscovite, chlorite, and calcite, whereas those of the amphibolite facies consist of quartz, epidote, and biotite.

D_2 in north-west Ghana is distinguished by extensional features caused by the collapse of some crustal thickened nappe (Block et al., 2016). This is characterized by a north-south down-dip oriented lineation, as well as the exhumation of lower crustal materials as seen in the Bulenga area. The contrasting metamorphic grades between migmatite and greenschist facies that is separated by a shear zone are one of the most compelling arguments for extension in this region.

The Wa-Lawra belt has been affected by D_3 regional scale N to NNW-trending transcurrent shear zones that have affected most of the volcanic and volcano-sedimentary units. It has also structured most of the syn-tectonic intrusion and early magmatic rock that formed around 2160 Ma (Baratoux et al., 2011). An S_3 vertical dipping penetrative metamorphic foliation parallel to primary bedding is associated with the D_3 event. These shear zones are primarily sinistral in nature.

D_4 deformation (Block et al., 2015) in north-west Ghana corresponds to regional D_2 of Baratoux et al. (2011) and consists of steeply dipping NNE to ENE oriented anastomosing dextral transcurrent S_4 shear zones with shallow dipping lineation. The majority of the D_4 shear zones are

located in upper greenschist facies. The S_4 shear zones are mostly brittle to ductile in nature, as opposed to the majority of S_3, which generally has ductile and schistose fabric. This implies that S_4 shear zones occurred at lower temperatures than D_3. Gold mineralization is associated to this deformational event.

The formation of crenulation cleavages and kink folds characterizes the regional D_5 (Block et al., 2015) deformational phase, which correlates to regional D_3 of Baratoux et al. (2011). S_5 space cleavage and kink folds mostly steepen, dip, and cross-cut the S_3 and S_4 foliations at high angles (Baratoux et al., 2011).

D_6 on the other hand, is characterized by late NE-SW steeply dipping faults. They are mostly observed in geophysical images. Block et al. (2015), describes the structural pattern of the D_6 to be consistent with the overall N-S compression. These faults were described as brittle and having less extension than the main transcurrent shear zones in D_3.

2.4 Gold deposits in the Paleoproterozoic Birimian in Ghana

This subsection is a summary of the features of gold deposits chiefly restricted within the Paleoproterozoic Birimian and Tarkwaian terranes of Ghana based on the general rock types, mineral paragenesis, structures and the ore body geometry. Figure 6 below shows the distribution of the gold deposits in Ghana.

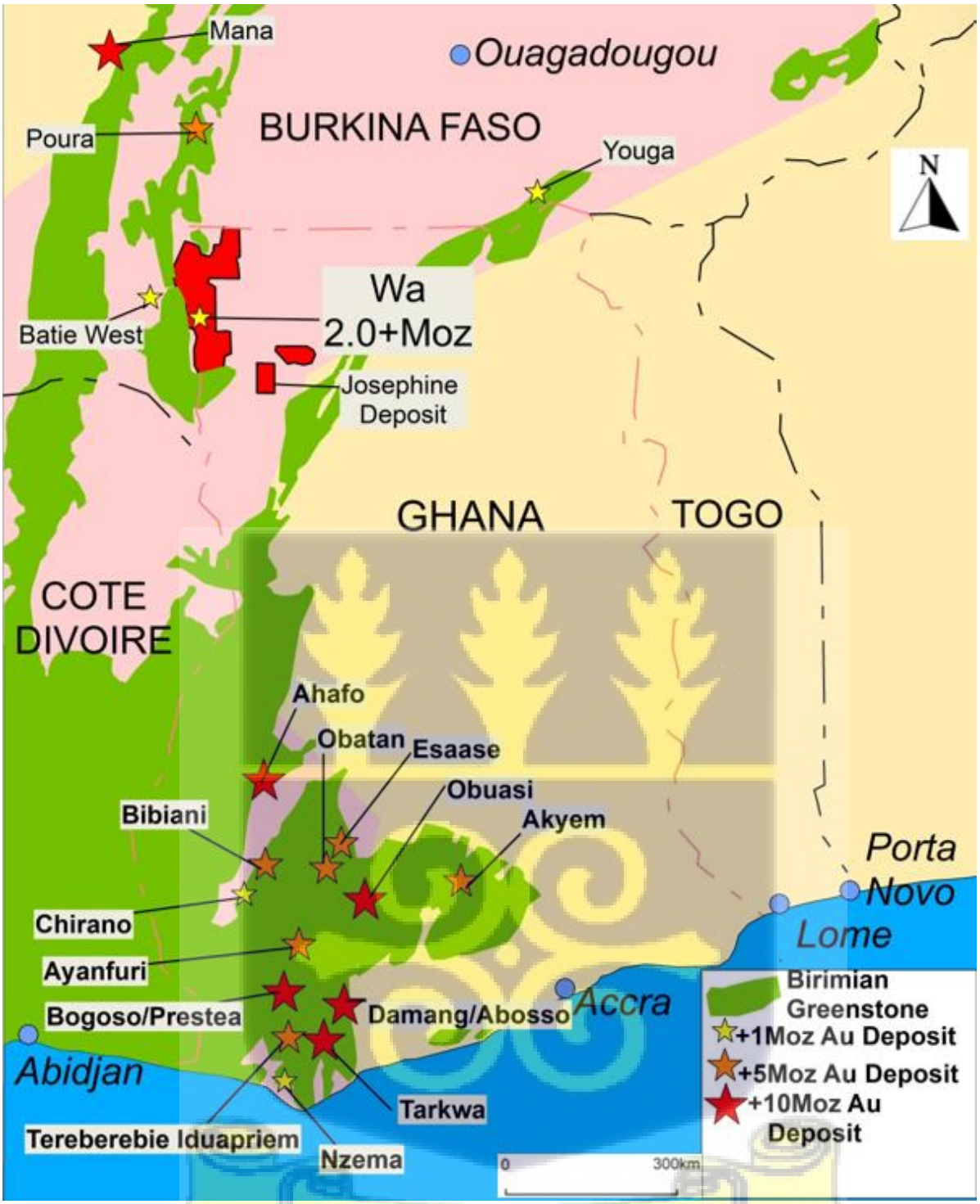

Figure 6. A Map of part of the Leo-Man shield of the West African craton showing the distribution of gold deposits and mines (modified after Milési et al., 2004). Insert in red is the Josephine deposit, a part of the Wa-Gold project owned by Azumah Resources limited which is the focus of this MPhil research.

Ghana has several gold deposits or mines, notable world class deposits among them are the AngloGold Ashanti limited Obuasi mines, the Wassa mines (Gold star Resources), the Konongo mines (Owere mines), Ahafo mines (Newmont Ghana limited), Damang and Tarkwa mines (Goldfields).

These world-class deposits can be found in a variety of lithologies, including metasediments (volcaniclastics, greywackes, shales, and chemical facies defined by cherts, manganese, and carbon-rich sediments), volcanics, and intrusive rocks. The deposits are usually found along or within the NE trending faults that defines the regional structural framework. The gold in these deposits is associated with disseminated gold bearing arsenopyrites and primarily occurs within metasedimentary rocks, as well as quartz veins and stock works associated with free gold and polymetallic sulphides such as arsenopyrite, galena, pyrrhotite, and chalcopyrite.

Gold found in the Tarkwaian in Ghana which is considered as a molass of paleoplacers of the Birimian terrane known as the Tarkwaian deposit. The gold is found in conglomerate rock. For instance, gold is mined in the Banket sequence or Tarkwaian reefs at the Iduaprem and Teberebe mines (AngloGold Ashanti Limited). Free gold is occasionally associated with iron-rich conglomeratic horizons. Also, Azumah Resource's Wa gold project (Fig.6) which is the focus of this research forms part of the deposits in the Birimian of Ghana. It is located on the Wa-Lawra belt and has a total resource of approximately 2.8 million ounces (Moz).

CHAPTER THREE

MATERIALS AND ANALYTICAL METHODS

In order to fulfil the set-out objectives, the work plan for this study was separated into three parts; desk study, field work, and laboratory analysis. The activities associated with each step are detailed in the following sections;

3.1 Desk Study

In order to have a fundamental and fair understanding of the subject area, a review of relevant literature (including pertinent books, scientific journals, and electronic databases) was performed. Azumah Resources Limited provided topographic maps, regional geology maps, and aeromagnetic data for the research area. These items greatly enable me prepare for the field work., Geological tools and materials were also obtained. The field work was undertaken in two field seasons. The first was between late October to the end of November in 2020 and the second; February to April in 2021.

3.2 Field work

The field work lasted for sixteen (16) weeks in total. The first field season was used mainly for structural and lithological mapping and representative rock sampling. The second field season was mainly used for drill core logging and completion of the structural and lithological map.

3.2.1 Reconnaissance Study

Reconnaissance study preceded the main field mapping. During this stage, a general assessment of the area was done for the purpose of self-familiarization with the field. All geological compasses were corrected, mapping pace was checked, and self-orientation and positioning were done at this stage.

3.2.2 Main Geological Field Mapping and Logging approach

Following the reconnaissance survey, systematic field mapping was undertaken at a scale of 1: 50,000km. Throughout the field study, GPS and compass method of mapping were employed. This approach is considerably more convenient, especially when mapping is done methodically. At every location in the field, the GPS displayed the position in terms of WGS 84 georeferenced coordinates. The GPS was also the only instrument utilized to record the geographical positions of all geological features (rocks and structures) found on the field. Because of this, the GPS-and-compass approach was used instead of the pace and compass and tape and compass methods.

Traversing was done in NW-SE direction across the general NE-SW strike direction. Detailed structural mapping was performed in areas previously drilled by Azumah resources LTD and areas determined to be faulted from the geophysics data in order to delimit the mineralization zones, understand the structural framework and to understand the hydrothermal plumbing system.

The initial tasks performed at each outcrop observation station is self-orientation, self-positioning and recording of geographic location/coordinates. Followed by these, was macroscopic and mesoscopic observation and description of the rocks to provide a "general view" of all geological characteristics. The rocks and structures were then closely examined and described in order to get details on all of the components that make up the totality of each geologic feature. The colour, the texture, orientation and size of the minerals as well as the location, structure, deformation, and metamorphism were all used to characterize the rocks. Petrographic description and data recording into the field notebook and map were completed. Relevant geometric properties such as orientation, size, shape, and position in time and space were used in plotting the lithologic units. The metamorphic study was by identifying specific minerals, which could give information on the grade of metamorphism.

Representative samples (40 samples in total) were collected for laboratory (thin section, SEM and whole-rock geochemistry) work. Of interest were mineralized, unmineralized, altered and unaltered (fresh rocks) samples. These samples were collected to help understand the mineralization and alteration of the area. Oriented samples were taken where possible, for microstructural analysis.

The borehole data, (rock chips) from reverse circulation (RC) drilling and diamond core drilling (DD) of the Josephine gold deposit were logged. This laid the groundwork for putting the recorded geological data into a three-dimensional framework, with lithological, structural and alteration constraints on gold mineralization. A total of 105 boreholes (RC and DD combined) were recorded in the Josephine deposit.

3.3 Laboratory work

The laboratory work involved preparation of thin-sections, analysis of petrographic and microstructures, Scanning Electron Microscope (SEM) analysis, and sample preparation for whole-rock geochemical analysis.

3.3.1 Sample preparation for thin sections and SEM

3.3.1.1 Thin section sample preparation

Thin-sections for thirty of the forty representative samples brought from the field were prepared at the petrological laboratory of the Earth Science Department, University of Ghana. A rock cutting machine (with a diamond edged blade) was used to cut the rock samples used for the thin-section preparation.

Thirty representative samples from the field were prepared for thin-sections, and were made at the Earth Science Department, University of Ghana.

The thin-section was cut across the foliation plane (if any) in each rock. The surfaces of the thin slabs were grinded and smoothed using silicon carbide powder. The smoothened surfaces of the blocks were mounted on 48x28 mm glass slides using Canada balsam. The remaining surfaces were polished and ground down using silicon carbide powder grade 80 till the rocks became thinner. As the portion got thinner, finer abrasives were applied. At a later stage of grounding, 600 silicon carbide powder was utilized until the rock thicknesses is 30 microns. The Leica DM750 P, laboratory petrographic microscope was used to ascertain whether the thickness of the thin section is appropriate for the microscopic studies by continuously observing the interference colours of minerals. After carefully removing extra cement, the pieces were covered with a glass cover-slip bonded with Canada balsam.

Thirty thin sections were produced and meticulously inspected for petrographic, textural, and microstructural characteristics using an optical polarizing microscope.

3.3.1.2 SEM sample preparation

Five (5) samples containing sulphides from the mineralized zone were selected, cut and polished into rounded shape with size and thickness of 20 mm and 10 mm respectively. The prepared samples were then mounted on aluminium platform ready for analyses using the scanning electron microscope to detect the main elements and minerals associated with the gold mineralization.

3.3.2 Petrographic and Microstructural Analyses

The petrographic examination of the 30 thin sections were carried out at the petrological laboratory of the Department of Earth Science, University of Ghana, using a polarizing light microscope (petrographic microscope). The petrographical descriptions of the thin sections were done descriptively as well as quantitatively. Textural description (including modal estimation of minerals, grain size of each mineral species, grain shape, inclusions of mineral grains, mineral

alteration, recrystallization, overgrowth and intergrowth textures and mineral associations, and the sulphides) and micro-structures were included in the quantitative description. Terry and Chilingar (1955) mineral estimation tables were used to calculate the modal percentages of the minerals under the petrographic microscope.

The identification of textural characteristics (including minerals and their proportion in the rocks) aided in determining mineral paragenesis, metamorphic conditions, and rock petrogenesis. The Amscope camera and program was used to take photomicrographs of the thin-section studied. Hand specimen description together with the thin section petrographic data enabled me assign appropriate names to the various rocks observed in the field.

3.3.2.1 Scanning electron microscopy analysis.

A Zeiss EVO MA15 SEM together with an energy dispersive X-ray spectrometer (Bruker Nano GmbH) and an XFlash Detector 610M was used to obtain images in backscattered electron mode (BSE) at the University of Mines and Technology, Tarkwa geological engineering laboratory. An acceleration voltage of between 16 kV to 21 kV was used to conduct electron scanning of various sulphides observed in the five (5) mounted thin sections within the mineralized zone to detect the minerals and elements associated with the gold mineralization.

3.3.3 Whole rock Geochemical Analysis

The following procedures were applied to allow for a successful whole rock geochemical analysis. This comprises sample preparation, analytical procedures, and data processing. Each of them is explored in detail in the segments that follows:

3.3.3.1 Sample Preparation

Ten (10) rock samples were sorted out of the thirty (30) samples used for the petrographic analysis, five each from the altered and unaltered zone. The selected rock samples were cut into uniform rectangular pieces of sizes 7 cm long, 5 cm wide, and 2.5cm thick. Unwanted parts of each rock, including weathered and inhomogeneous pieces, were removed to assure rock homogeneity and the dependability of geochemical data. The samples were labelled appropriately, packed into a box, and transported to ALS laboratory in Kumasi, for onward transmission to their laboratory in Canada, where the geochemical analysis was performed.

3.3.3.2 Analytical Techniques

The samples were subjected to major and trace element analyses using Inductively Coupled Plasma Atomic Emission Spectrometry (ICP-AES) and multi-elements fusion Inductively Coupled Plasma Mass Spectrometry (ICP-MS), respectively. At 1000°C, the loss on ignition was calculated.

For major element analysis, a combination of 0.200g of prepared samples and lithium metaborate was fused in a furnace at 1025°C. The resulting melt was then cooled and dissolved in a nitric, hydrochloric, and hydrofluoric acid combination. ICP-AES was then used to examine this solution for the main element composition of the different rocks.

The trace element analysis laboratory techniques were the same as those observed for major element analysis. The prepared samples for trace element analysis, on the other hand, weighed 0.100g and were analysed using the ICP-MS. For base metal analysis using ICP-AES, 0.25g of prepared sample was digested with perchloric, nitric, hydrochloric, and hydrofluoric acids. The residue was then treated with diluted hydrochloric acid, and the solution was evaluated using the ICP-AES. The acquired results were adjusted for spectral interferences. Precision is more than 2%.

3.3.3.3 Data Analyses

To quantitatively evaluate the chemical gains and losses during the hydrothermal activity on the Josephine deposit, the major-oxide and trace-element compositions obtained by whole-rock geochemical studies was used. The Grant (1986) isocon technique was applied to assess substantial changes in composition, mass, and volume. These mass, volume and compositional changes were calculated using the EASYGRESGRANT MS-Excel sheet and following the procedures as describe in Lopez-Moro (2012)

CHAPTER FOUR

RESULTS

This chapter describes the field and laboratory observations using multiple figures, tables and maps to illustrate the findings of this work. This will be organized into six major subheadings namely; (i) lithological description, (ii) structural features and deformation (iii) alteration, (iv) ore body characteristics and geometry (v) Isocon analysis and (vi) ore mineralogy.

4.1 Lithological description and metamorphic mineral assemblages

In this segment, the various rocks types are described based on the field observation, hand specimen description and thin section analysis.

4.1.1 Lithological description

From careful and systematic field and laboratory studies of the various rock samples, rocks in the study area are categorized into strongly sheared granitoid (three types; granite, granodiorite and diorite), quarzitic rocks (quartzite and quarzitic schist), gneiss and dolerite. The distribution of the major rock outcrops is shown on the outcrop map (Fig. 7) using their geometric features; size, shape, orientation, position in space and time with respect to scale. The mineralogical composition and modal percentages of the various rocks are also shown (in Table 1).

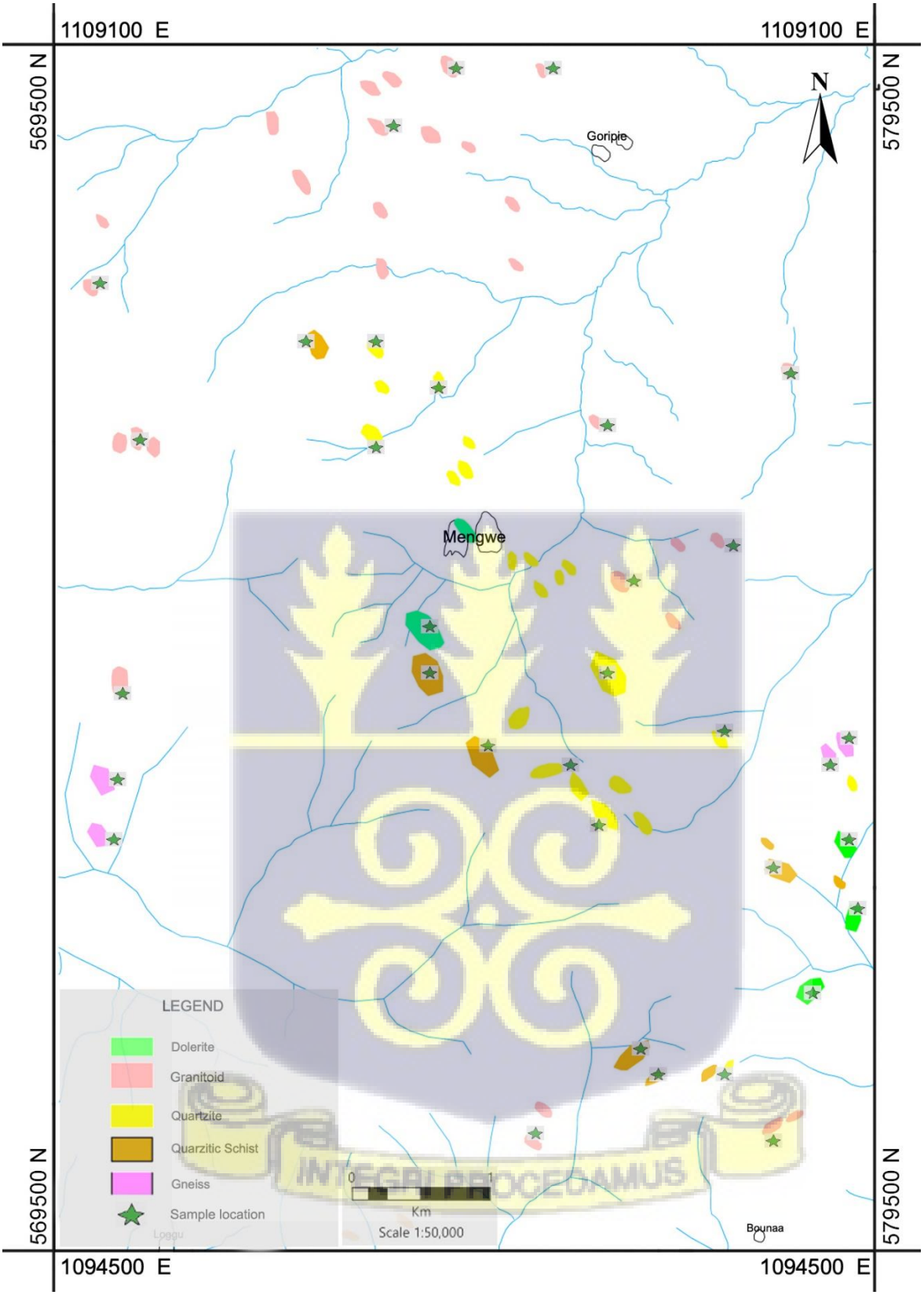

Figure 7. Outcrop map showing the distribution of the various rock types in the study area.

Table 1: Mineralogical composition of granitoid using visual estimation charts after Terry and Chilingar (1995).

	Modal composition (%)						
	Granitoid			Quarzitic rocks			
Minerals	**Granodiorite**	**Granite**	**Diorite**	**Quartzite**	**Quarzitic schist**	**Dolerite**	**Gneiss**
Quartz	20	30	15	80	70	5	30
Plagioclase	35	25	30	2	2	40	20
Microcline	5	10	<1	<1	<1	<1	<1
Orthoclase	20	20	5	3	3	2	25
Biotite	5	5	15	3	7	5	15
Muscovite	3	2	5	2	5	3	3
Sericite	5	1	1	2	2		-
Amphibole	3	-	20	-	-	15	3
Pyroxene	-	-	-	-	-	20	-
Epidote	<1	-	-	<1	-	-	
chlorite	2	3	5	2	3	4	2
Titanite	-	-	1	-	-	-	-
Calcite	<1	-	<1	-	-	-	-
Sulphides	-	2	2	3	3	-	-
Magnetite	<1	<1	<1	2	2	5	2
Garnet	-	-	-	1	2	-	-

4.1.1.1 Granitoids

The investigated plutonic rocks herein generally termed granitoid, can be separated into three distinct rock types: granodiorite (Fig. 8a), granite (Fig. 8b) and diorite (Fig. 8 c-d). The granitoid in the study area occurs mostly at the north-eastern part, southern and western portions of the study area.

Granodiorite

In hand specimen, the granodiorite is leucocratic, phaneritic in texture and is predominantly composed of about 20% quartz, 35% plagioclase, 20% k-feldspar (orthoclase), minor amounts of sericite (5%), and amphibole (3%), with magnetite as accessory mineral (estimated mineral abundance shown in table 1 above). Thin section analysis revealed that the granodiorite is holocrystalline has hypidiomorphic-granular texture (Fig. 9a). plagioclase and amphibole appear euhedral while k-feldspar, quartz and sericite are subhedral.

Granite

Hand specimen analysis revealed that the granite is also leucocratic and composed of about 30% quartz, 29% plagioclase, 25% k-feldspar, muscovite and sulphites as accessory mineral. The granite (Fig. 9b) is holocrystalline and composed of subhedral quartz, k-feldspar, plagioclase, muscovite and sulphides making it hypidiomorphic-granular in texture. Plagioclase, k-feldspar shows their characteristic polysynthetic twinning and Carlsbad twinning under cross polar lights but appear colourless under plane polar lights. Quartz is colourless under plane polar light and exhibits undulous extinction under cross polars while the sulphide maintains its black colour both in cross polar and plane polar lights and is cubic in shape.

Diorite

Diorite is mesocratic, has a phaneritic texture and composed of 30% plagioclase, 15% quartz, 20% hornblende, 15% biotite with pyrite and muscovite as accessory mineral.

Mafic xenoliths (Fig. 8c) were a common occurrence in the diorite rocks. Shearing, and veining (Fig. 8d) is also common in all the diorite. Also observed in the rocks is chlorite alteration, which is frequently observed in rocks with sulphides. In this section, the texture of the diorite is allotriomorphic granular and it is also holocrystalline. Quartz, k-feldspar, biotite and chlorite are anhedral in shape while hornblende and sulphide (pyrite) appear idiomorphic with euhedral shape. Plagioclase and potassium feldspar have altered and into muscovite and sericite while biotite and hornblende have altered into chlorite.

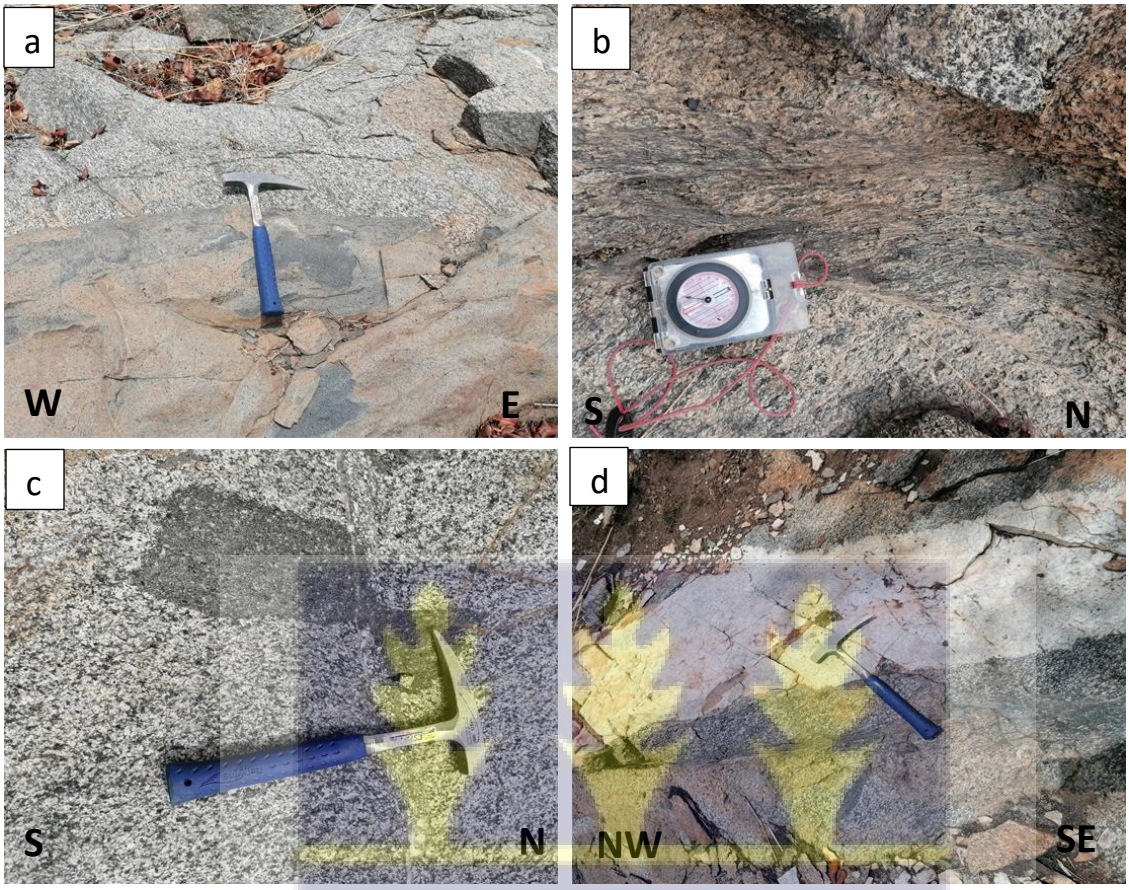

Figure 8. Field photographs illustrating the outcrops encountered in the study area (a) granodiorite (b) granite showing shearing (c) diorite with mafic xenoliths and (d) veining in diorite.

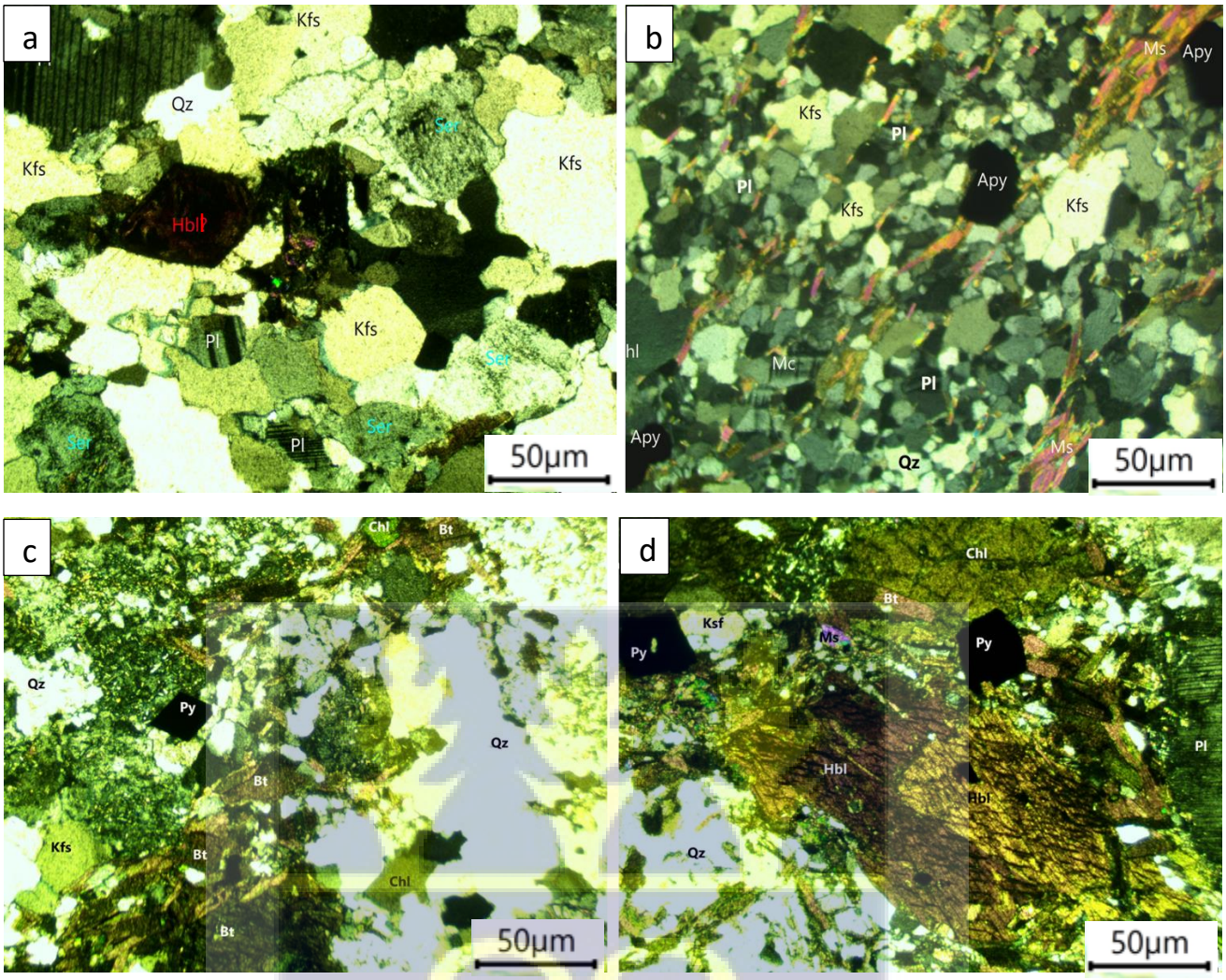

Figure 9. Photomicrographs showing (a) hypidiomorphic-granular texture, (c and d) pyrite and idiomorphic hornblende: Note the association between biotite and arsenopyrite (d) (crossed polars). Qz=quartz, Bt=biotite, Kfs=k-feldspar, Apy= arsenopyrite, Py=pyrite, Chl=chlorite, Hbl=hornblende, ms=microcline Ser=sericite. pl=plagioclase,

4.1.1.2 Quarzitic rocks

The quarzitic rocks observed in the study area are mainly two types; quartzite and quarzitic schist. They occur with the middle portion of the study area and the part of the southern portion.

The **quartzite** (Fig.10 a and b) is grey in colour, medium grained and composed of about 80% quartz, 5% feldspar (plagioclase and k-feldspar), minor biotite (3%), sulphides (3%) muscovite (2%), as well as chlorite (2%) and magnetite as a metamorphic mineral. The **quarzitic schist**

(Fig.10 c and d) is also grey in colour and composed of 70% quartz, 7% biotite, 5% muscovite, 3% sulphides and 3% chlorite (see details of mineral abundance in table 1). Both the quartzite and quarzitic schist exhibit some form of shearing. The shearing intensity within quarzitic schist outcropping in the southern portion of the study area increase significantly with the rock exhibiting schistose textures. Their schistosity is marked mica growth and parallel alignment of the platy and lath shaped mineral constituents. Primary sedimentary planar/tabular cross stratification are preserved in the quartzite (Fig. 10a) but are missing in the quarzitic schist. The rocks exhibit clear L-S tectonite fabrics (thus both flattening and elongated strains) such as mineral and stretching lineation (Fig. 10b), folding (Fig. 10c), boudinage quartz vein (Fig.10d), and shear planes. Joints are also common planar features observed in the rocks. Chlorite and magnetite are ubiquitous in the quartzites.

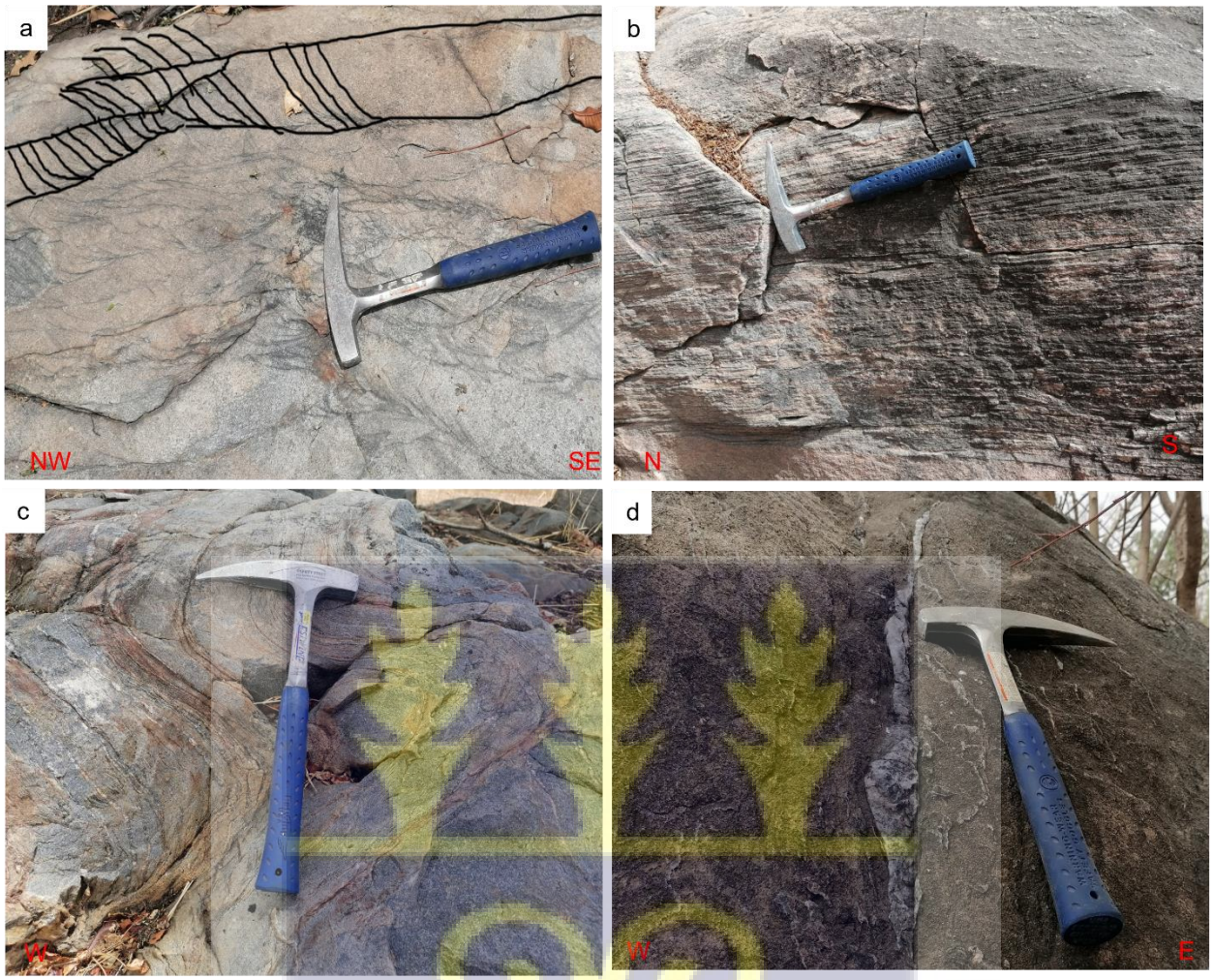

Figure 10. Field photograph of quarzitic rocks showing (a) tabular cross stratification in quartzite (b) mineral stretching lineation in quartzite (c) folding in quarzitic schist and (d) boudinage quartz vein quarzitic schist

Thin section analysis shows varying textures associated with the quartzite and quarzitic schist. These are porphyroblastic textures where the mineral biotite surrounds a deformed poikiloblastic K-feldspar with quartz and biotite inclusion associated with quartzite (Fig. 10a), granulitic texture in the quartzite (Fig. 10b) and schistose texture associated with the quarzitic schist (Figs. 10c-f). The sulphides are opaque in colour and cubic and monoclinic shaped and occur along the foliations

together with the micas (Figs. 10c-f). The rocks display penetrative metamorphic foliation which comprises oriented white mica, biotite, and quartz.

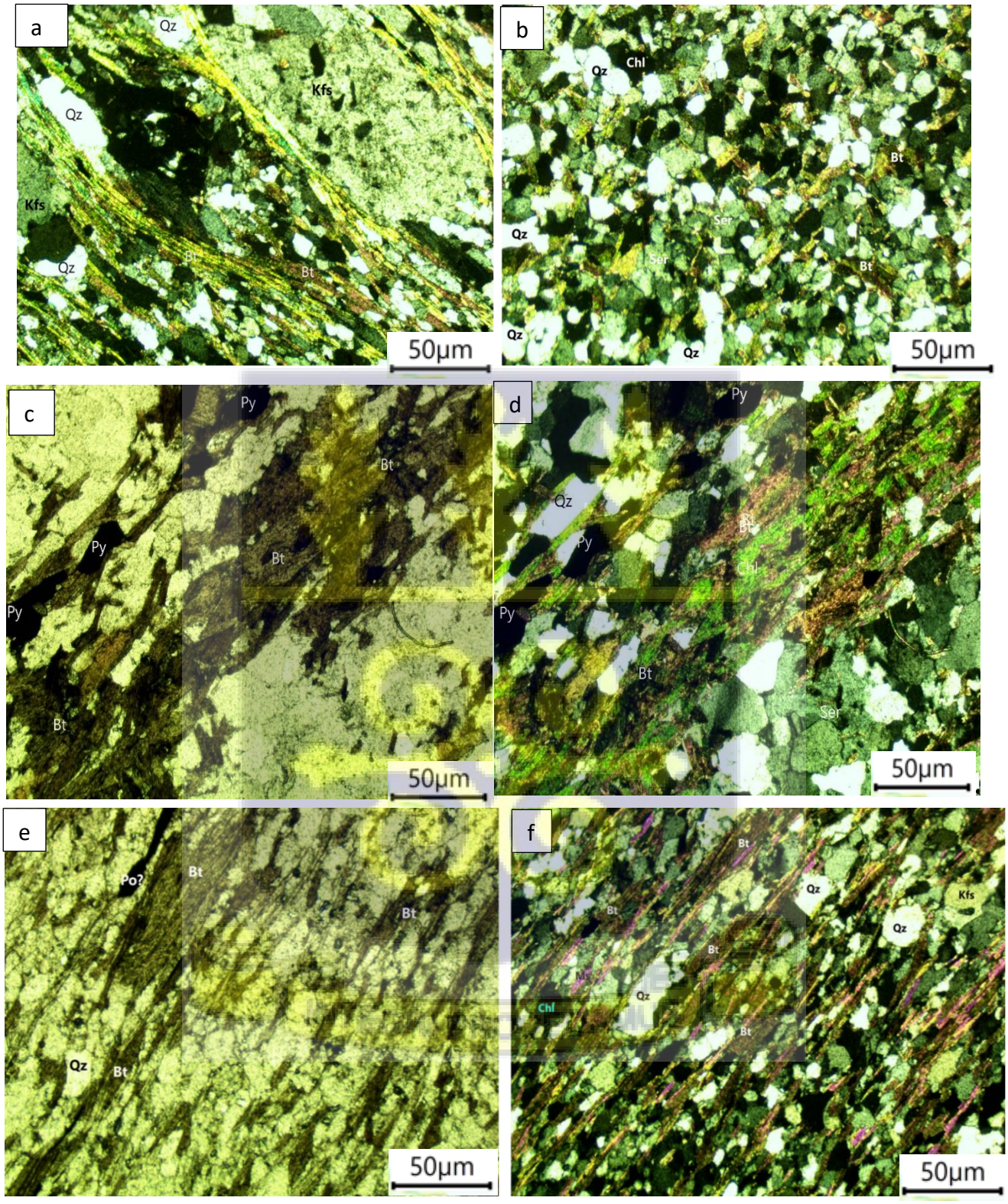

Figure 11. Photomicrographs of quartzite showing porphyroblastic texture (a), granulitic texture (b) and schistose texture (c to f), a, b, d and f are takem in crossed polars while c and e are taken in plane polars. Qz=quartz, Bt=biotite Chl=chlorite, Py=pyrite, Po=pyrrhotite Kfs=K-feldspar

4.1.1.3 Dolerite

A Plutonic and hypabyssal intrusive rock (dolerite sill) was observed in the study. They occur in the central and south eastern portion of the study area and are seen intruding the granitoid at central part of the study area (Fig 12a). The dolerites are dark green in colour, fine to medium grained, mostly sheared, highly magnetic and composed of 40% plagioclase, 15% amphibole, 20% pyroxene and 4% chlorite with 5% quartz and magnetite as accessory minerals. Quartzo-feldspathic veining was also observed in the dolerite (fig. 12b).

Figure 12. Field photographs showing dolerite sill intrusion in granitoid (a) quartzo-feldspathic veins (b)

Thin section analysis revealed that the dolerite is hypo-crystalline and sheared as observed by the elongation of minerals (Fig.13a.), with plagioclase showing subophitic and lath shape textures (Fig. 13b). Plagioclase, clino-and-ortho-pyroxene, hornblende, biotite chlorite and some opaque

minerals are the minerals observed under thin section. The plagioclase occurs as short prismatic crystals with a polysynthetic twinning. The clino-pyroxenes, mostly augite, is more abundant than the ortho-pyroxene (Fig. 13c). Alterations are common, as indicated by the alteration of plagioclase to sericite and clay and biotite to chlorite.

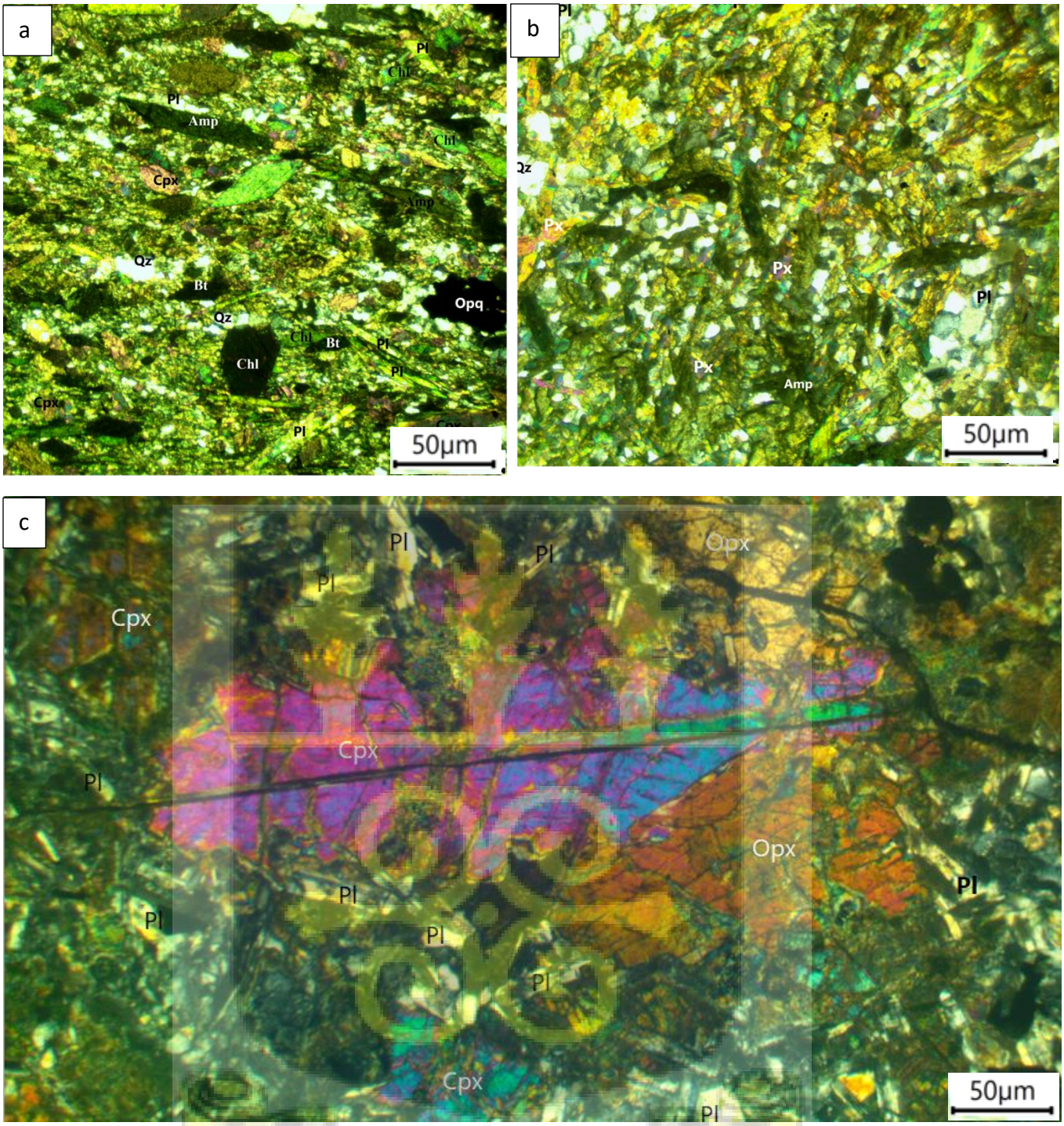

Figure 13. Photomicrographs showing shearing in dolerite (a) mineral elongation (b), and clino-and-ortho-pyroxene as well as sub-ophitic texture (c) (crossed polars) Qz=quartz, Pl=plagioclase, Amp=amphibole, Px= pyroxene Cpx=Clinopyroxene, Opx=Orthopyroxene Chl=chlorite, Bt=biotite Opq=opaque mineral.

4.1.1.4 Gneiss

Gneissic rocks are observed to the south eastern and south western parts of the area where metamorphism is visibly high. The gneisses do have alternating leucocratic and melanocratic colours as a result of obvious typomorphic textures. They are coarse grained and generally composed of 15% biotite, plagioclase, 25% K-feldspar, 30% quartz, 3% amphibole, with minor chlorite (2%) and magnetite (2%) as accessory mineral. The melanocratic part of the banding in the gneiss is composed of minerals such as amphibole and biotite while the leucocratic portion is made up of plagioclase, quartz, muscovite and sericite. (Fig. 14a).

Under thin section, biotite appears elongated and surround plagioclase (Fig. 14b). Some of the minerals present, are quartz and K-feldspar with other minor and accessory phases including amphibole (hornblende), muscovite, and sericite. In plane polarized light, the k-feldspar(orthoclase) is colourless, the quartz and plagioclase are also colourless but biotite has a general pale brown colour and amphibole appear greenish. However, under crossed polarized light, the orthoclase shows simple Carlsbad twins and perthitic texture (Fig. 14c), plagioclase exhibit polysynthetic twins, amphibole show imperfect cleavage planes at 54° and 124° and quartz shows undulous extinction. The orthoclase and amphibole appear subhedral in shape whiles the plagioclase has euhedral mineral grains. The biotite is however, tabular and elongated along the foliations (Fig. 14b). The foliated texture of gneiss is defined by the preferred oriented and elongated biotite crystals usually sharing grain boundaries with quartz mineral (Fig. 14b). Some quartz and orthoclase crystals exhibit micro-fractures. The feldspars in the rock show evidence of some form of mineral alteration.

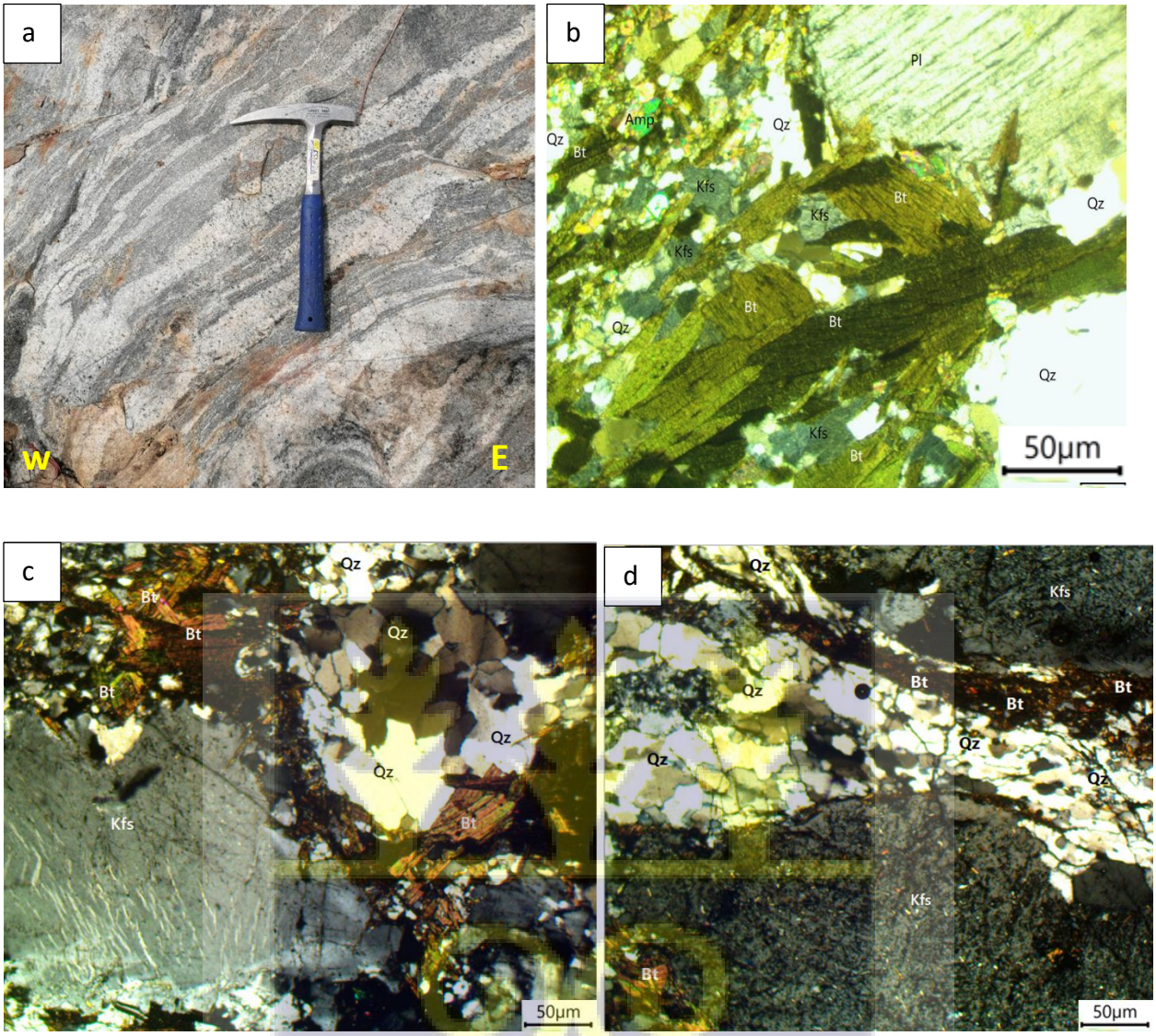

Figure 14. (a) Field photograph of gneiss showing gneissic banding, (b) photomicrograph of the mineral assemblage within the gneissic rock in the study area, (c) perthitic texture in porphyroblast k-feldspar and quartz showing undulous extinction (d) k-feldspar porphyroblast with inclusions and stretched quartz (crossed polars) Qz=quartz, Pl=plagioclase, Amp=amphibole, Kfs= K-feldspar, Bt=biotite

4.2 Structural features and Deformation

Careful and comprehensive analysis from lithological, structural mapping and drill core logging of rocks on the Josephine deposit has revealed a high degree of structural complexity in the study area. These structures are formed as a result of deformational (tectonic) and metamorphic processes that have influenced the terrain on macroscopic, mesoscopic, and microscopic scales. The terrane's higher level of structural complexity was revealed by careful and systematic structural and lithological studies. This structural work has allowed for the identification of four deformational events on the deposit. These are connoted as $D_{JO0,}$ D_{JO1}, D_{JO2} and $D_{JO3,}$ where the addendum JO denotes the local deformation as pertained to the Josephine deposit. The various deformational regimes are described vis-a-vis the structures that are associated with them. The kinematic indicators associated with each deformation is also presented accordingly. The general distribution and geometric attributes of these structures as well as tectonic fabric interpreted from aeromagnetic and electromagnetic data are displayed on the structural map (Fig. 15).

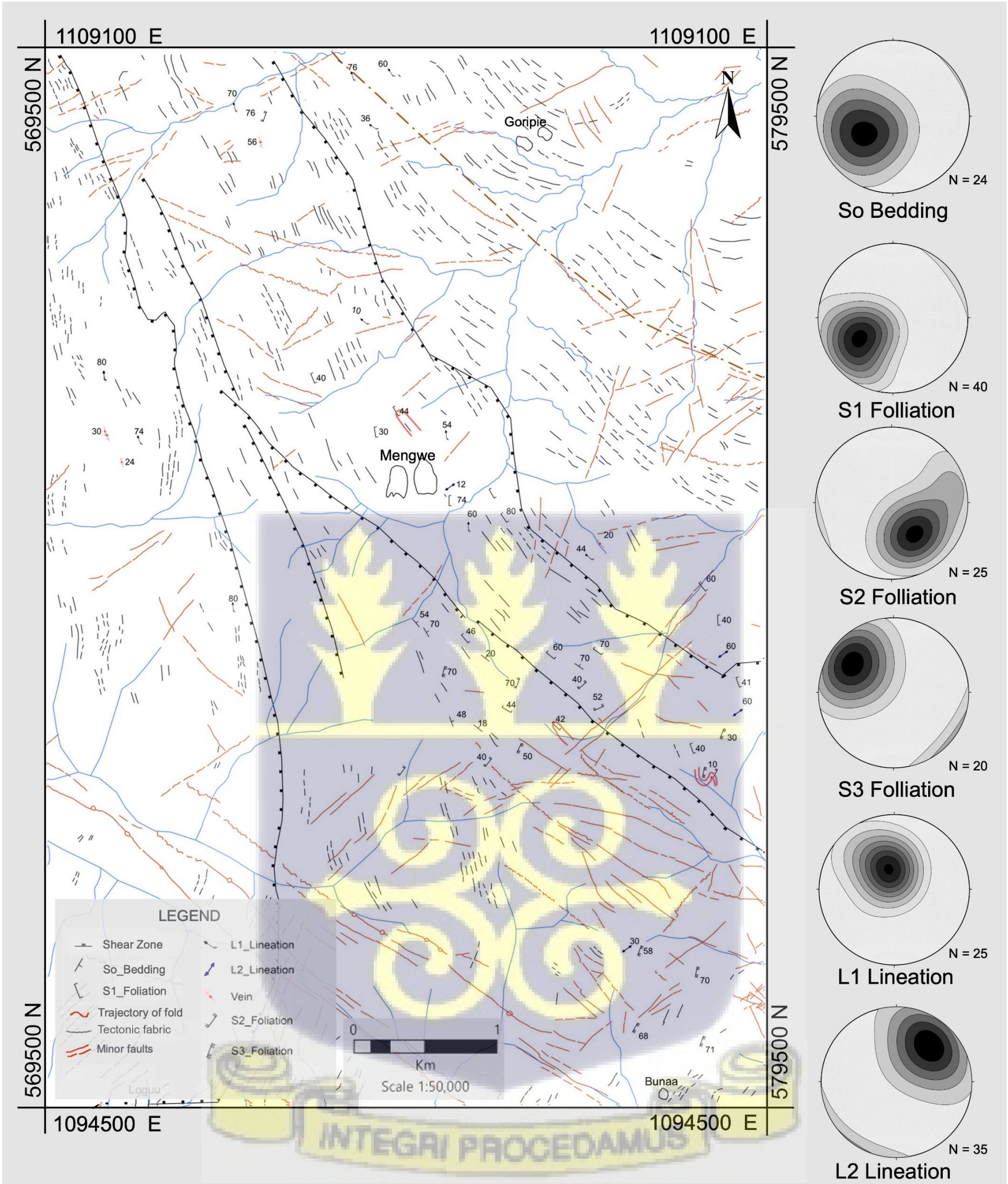

Figure 15. A simplified Structural map of the study Josephine deposit compiled from field measurements and structural fabric interpreted from geophysical data. Inserts are lower hemisphere stereographic projection for poles of the different deformational generation of foliation and lineaments.

4.2.1 D_{JO0} Deformational Regime

D_{JO0} in the Josephine deposit is associated with a shallow-to steeply dipping $S_{JO0,}$ represented by preserved planar/tabular cross stratigraphic layering of low-grade meta-sediments (quartzites). They are observed in the central part of the study area (Manwe). The general bedding (S_{JO0}) direction is NW-SE with steep dips in the NE direction as shown in the field photograph and Schmidt plot in Fig.16a and b respectively below.

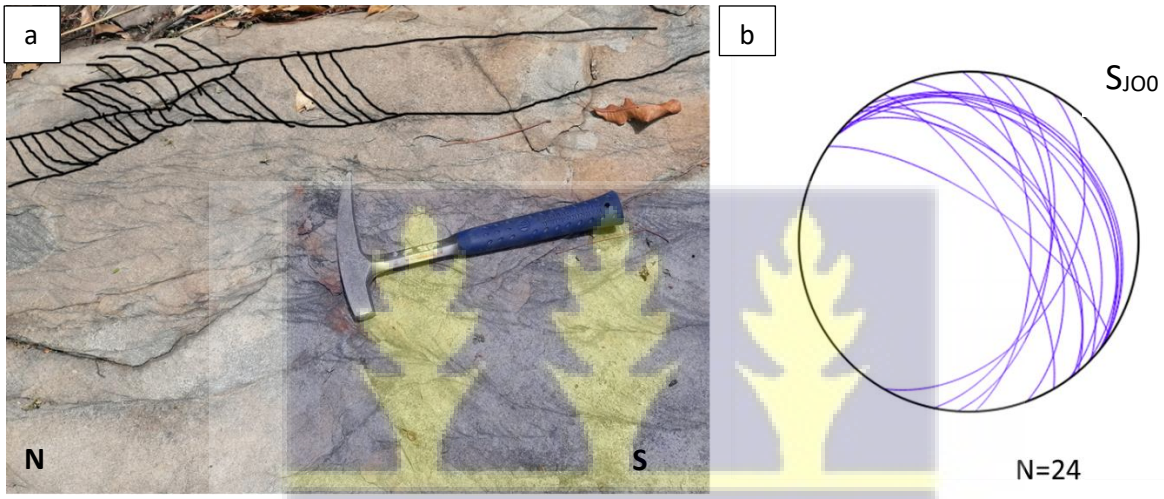

Figure 16. Field photograph illustrating (a) preserved sedimentary layering (cross bedding) and (b) an inserted Schmidt plot showing the general trend of the beds.

4.2.2 D_{JO1} Deformational Regime

D_{JO1} event is the most prominent deformational event and has affected almost all the rocks in the study area. D_{JO1} is associated with steeper more NNW trending 40 km shear zone with a generally NE-dipping sequence. This shear zone is defined by aright-stepping relay or dilatationl jogs with a dextral sense of movement as well as right lateral faults (Riedel shear) that is gently inclined into the main S_{JO1} shear foliation. This deformational regime is also associated with a shallow- to steeply dipping S_{JO1} penetrative shear foliation known as right-stepping relay or sinusoidal shear bend (dilational jogs), parallel to the S_{JO0} bedding with lineation (L_{1JO1}) plunging down-dip (Fig. 17 a,b). This shallow-steep dips on the shear zone defines a hanging and a foot wall sequence on the shear zone. The steep dips are the footwall and the shallow dips are the hanging wall. S_{JO1} foliation has a top-to-the-NE kinematic indicators with downdip plunging lineation. S_{JO1} shear foliation is defined by the axial planes of the F_{JO1} isoclinal folds with axial planes striking in the NW-SE direction with steep dips to the NE direction as shown below (Fig. 17 c,d).

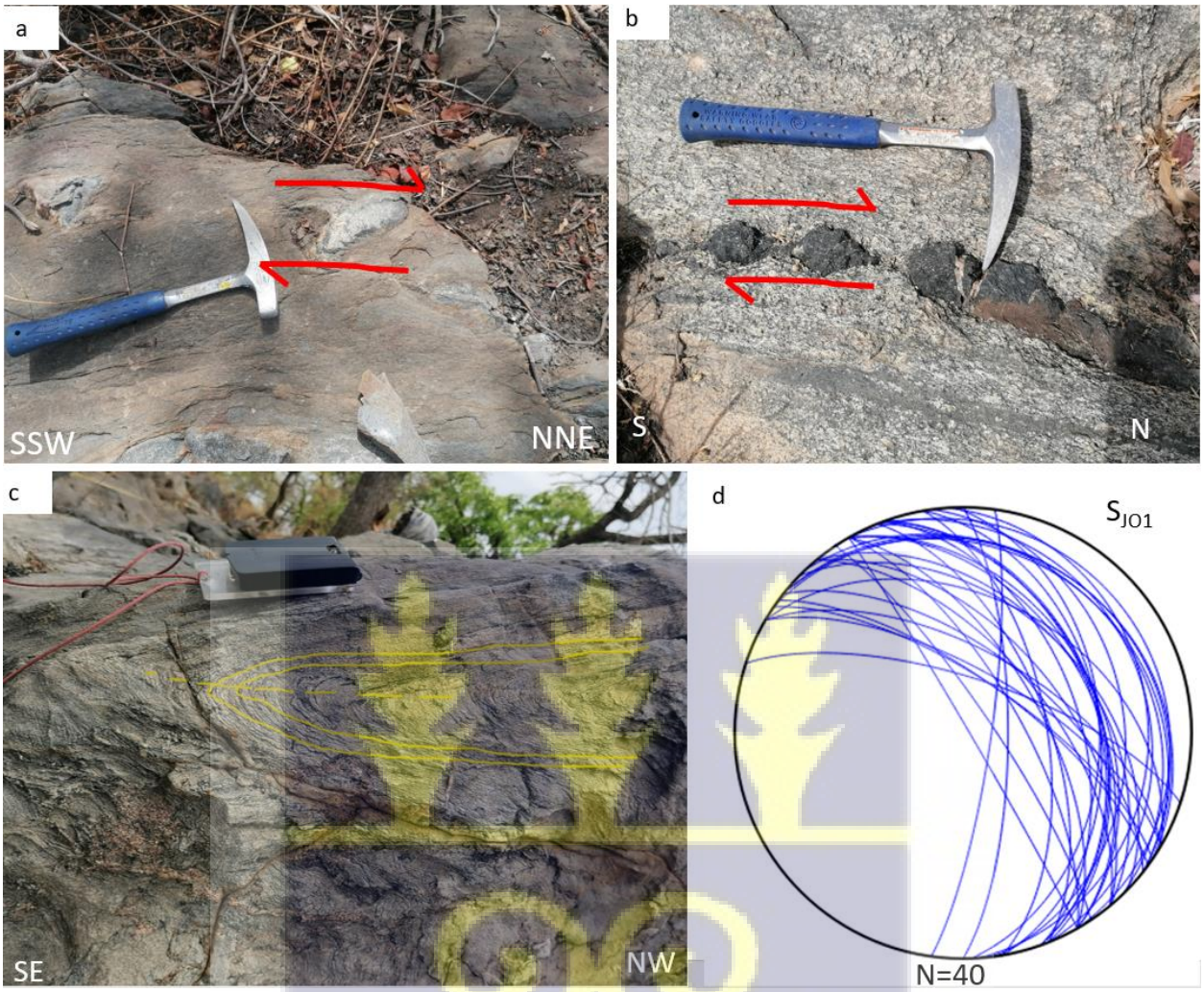

Figure 17. Field photographs showing (a, b) S_{JO1} foliation and boudins indicating the top-to-the-NE kinematic indicator and dextral sense of movement (c) F_{JO1} isoclinal folds defining the S_{JO1} foliation and (d) an inserted Schmidt plot showing the general dip and trend of the S_{JO1} foliation.

4.2.3 D_{JO2} Deformational Regime

D_{JO2} is characterized by a NE-SW striking foliation (S_{JO2}; Fig. 18a, b) whose dips ranges from 40°-70° to the north-west and has a stretching lineation (L_{JO2}) trending NE-SW ($L_{JO2,}$ plunging to N250-350) which plunges (40-70°) down-dip to the. D_{JO2} is also defined by F_{JO2} open folds (Fig.

18a). These could be observed in the meta-sediments and granitoid intrusions. In the field, there is no observable overprinting relationships between D_{JO1} and D_{JO2} structures.

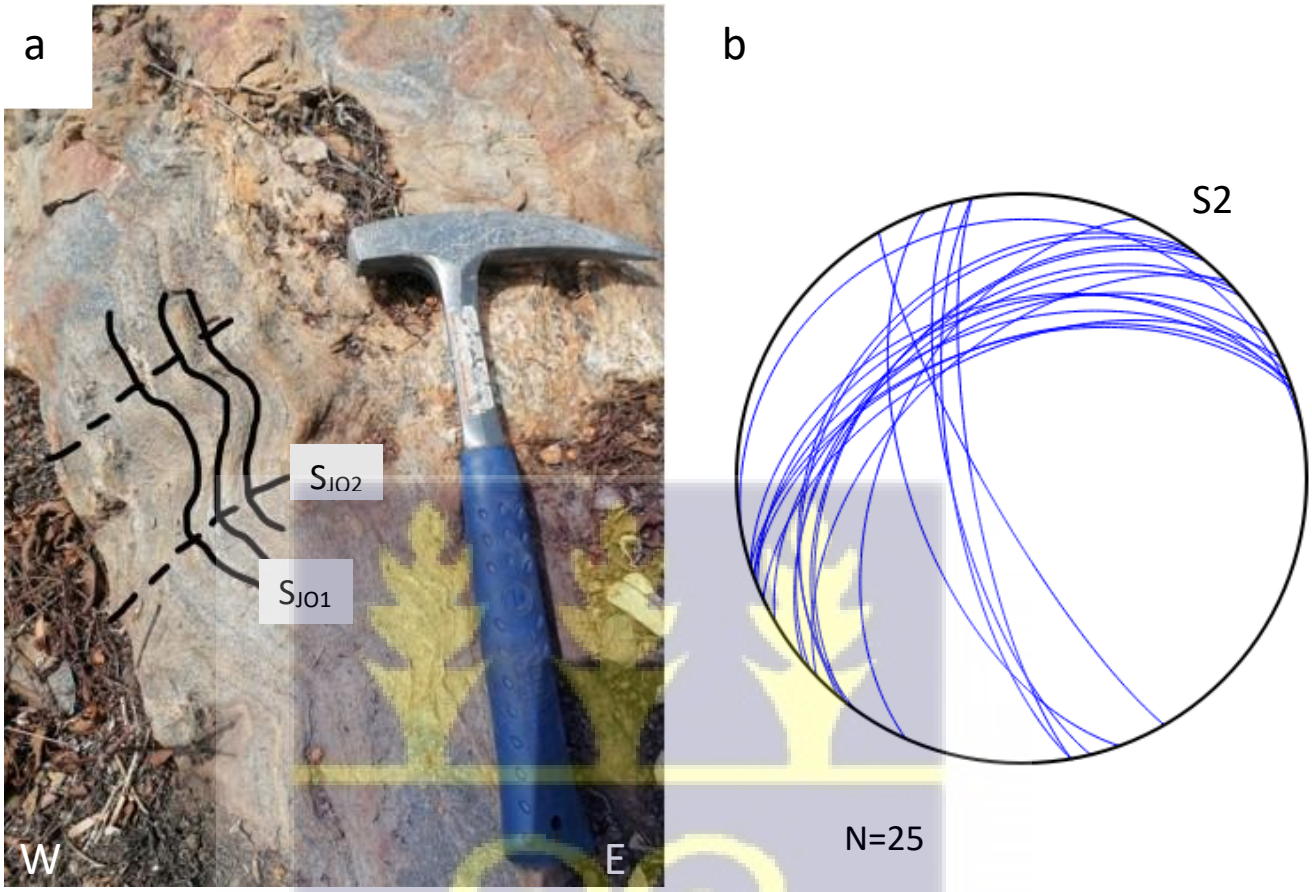

Figure 18. Field photographs illustrating (a) the relationship between S_{JO1} and S_{JO2} foliation. S_{JO2} foliation is defined by F_{JO2} open fold (b) inserted Schmidt plot showing the general dips and trend of the S_{JO2} foliations.

4.2.4 D_{JO3} Deformational Regime

The final stage of deformation D_{JO3} in the Josephine deposit is a brittle-ductile deformation which is associated with an NNE-SSW S_{JO3} foliation (schistose cleavage), and dextral faulting (Fig. 19a, b). At the southern part of the study area where there are high grade metamorphic rocks (Quarzitic schist of amphibolite facies), S_{JO3} forms a penetrative foliation and is axial planar to ptygmatic folds, F_{JO3} folds (Fig. 20a, b). D_{JO3} deformation is associated with an amphibolite-facies

metamorphic overprint. The Fabrics, structures and isograds formed during D_{JO1} and D_{JO2} are overprinted by D_{JO3} deformation, which is consistent with E-W directed horizontal contraction. In the NW portion of the Josephine deposits, E-W space cleavages have been observed in the granitoid (Fig. 20d).

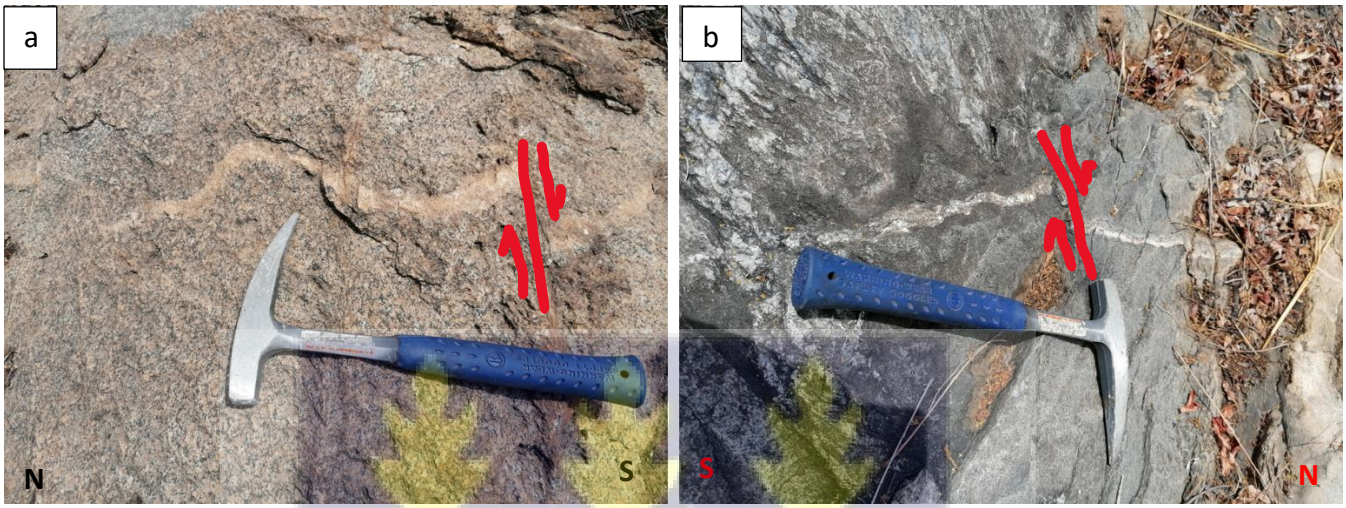

Figure 19. Field photographs illustrating dextral faulting associated with the final stage of deformation, D_{JO3}.

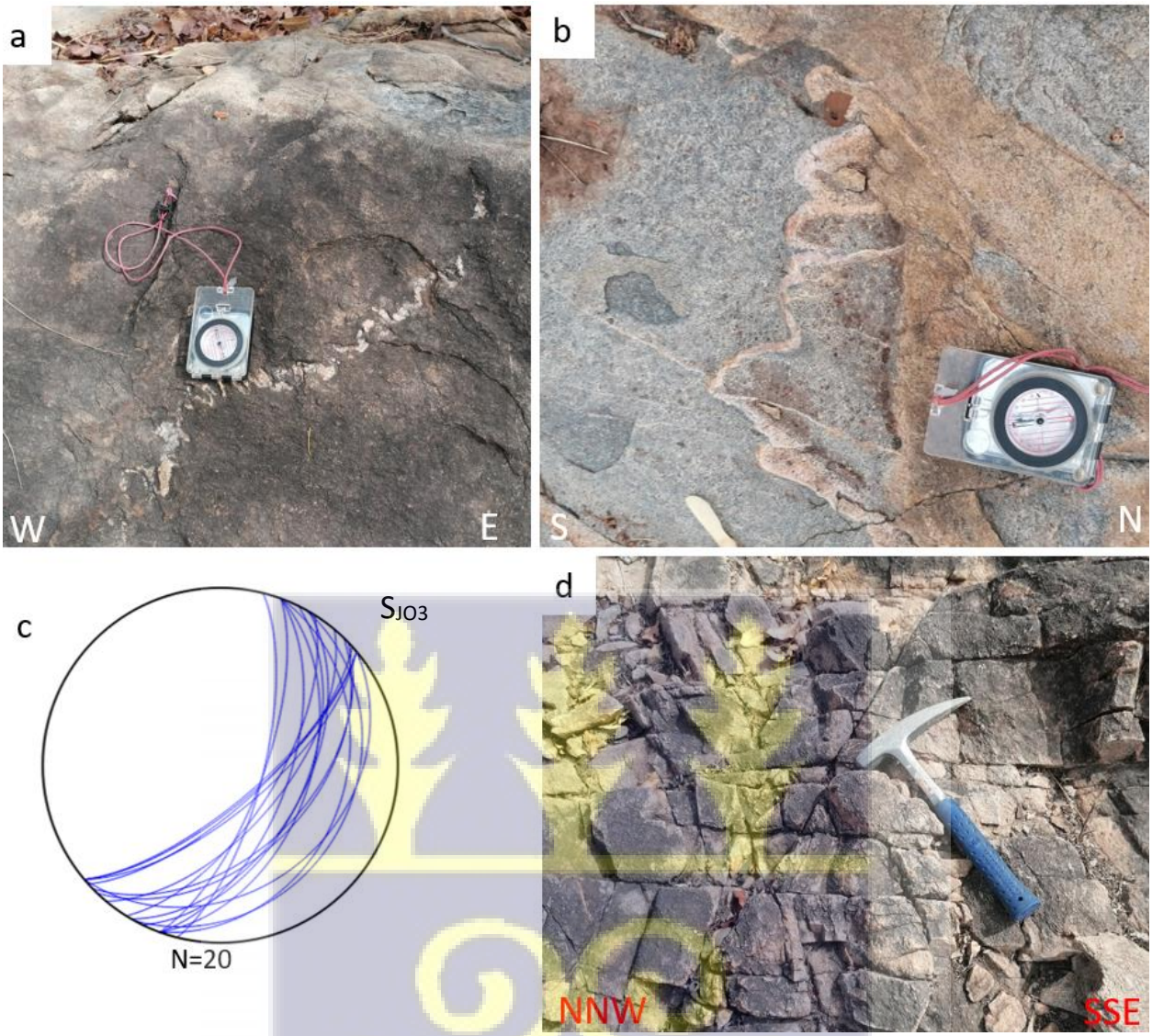

Figure 20. Field photographs illustrating (a, b) ptygmatic folding interpreted to represent the third generation of folding associated with D_{JO3} deformation, (c) inserted Schmidt plots illustrating their dip and trend of S_{JO3} foliation and (d) E-W space cleavages formed as a result of E-W directed horizontal contraction observed in the granitoid.

4.3 Alteration

In the Josephine deposit, mineral alteration could be observed both in the field and in drill cores. The diagnostic features of the altered zone which make it easily distinguishable from the unaltered

zone is bleaching of the rock (due to the intense silicification associated with the mineralized zone) as well as its mineral constituents.

Typically altered rocks are mostly greenish in colour and very hard. The mineral assemblage associated with the altered (mineralized) zone are chlorite + sulphides + sericite + quartz (silicification) (Fig. 21 and 22). The greenish colour associated with the altered zone is as a result of chloritization while the silicification results in the hardness of the rocks. Barren rocks may have greenish coloration (mostly less intense) and hard but lacks sulphides. Minerals such as feldspars and micas also alter into sericite (sericitization). The sulphides present in the altered zone are arsenopyrite, pyrite, and chalcopyrite, with the arsenopyrite being dominant (usually 3-5% intensity within the mineralized zone) and occur as disseminated grains.

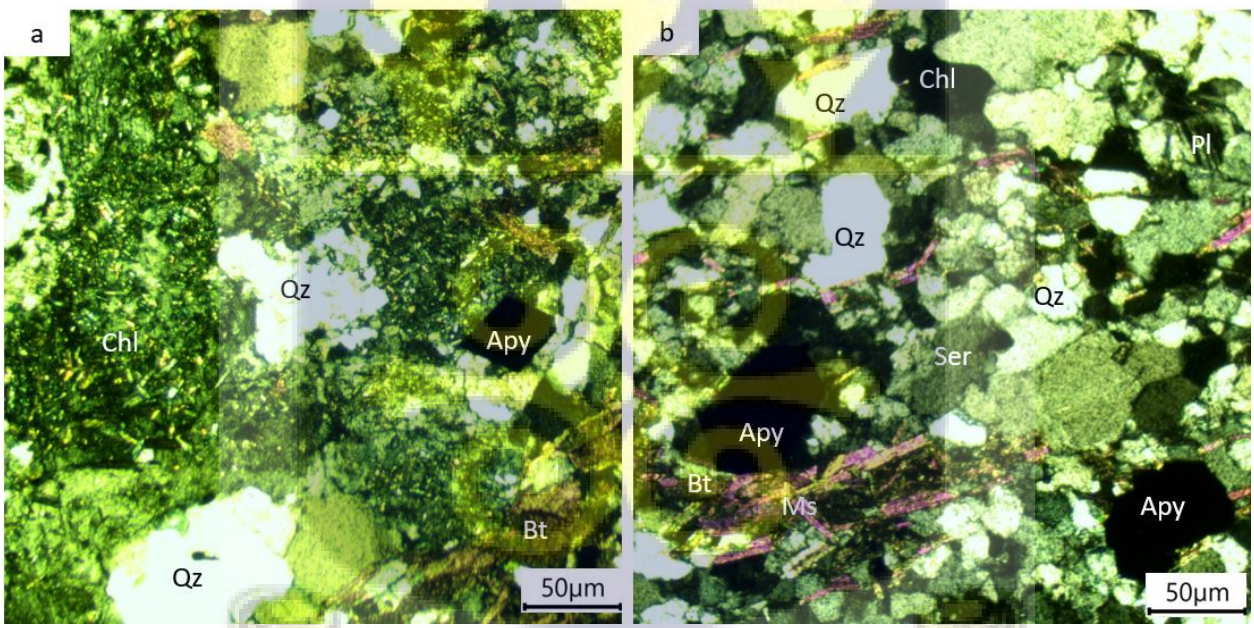

Figure 21. Photomicrograph showing the alteration mineral assemblage in the ore zone (a) shows the alteration mineral assemblage of quartz, chlorite and arsenopyrite with minor biotite (b) shows alteration mineral assemblage of quartz, sericite and arsenopyrite with minor micas. Qz=quartz, Ser=Sericite, Pl=plagioclase, Ch=chlorite, Bt=biotite Apy=Arsenopyrite, Ms=muscovite,

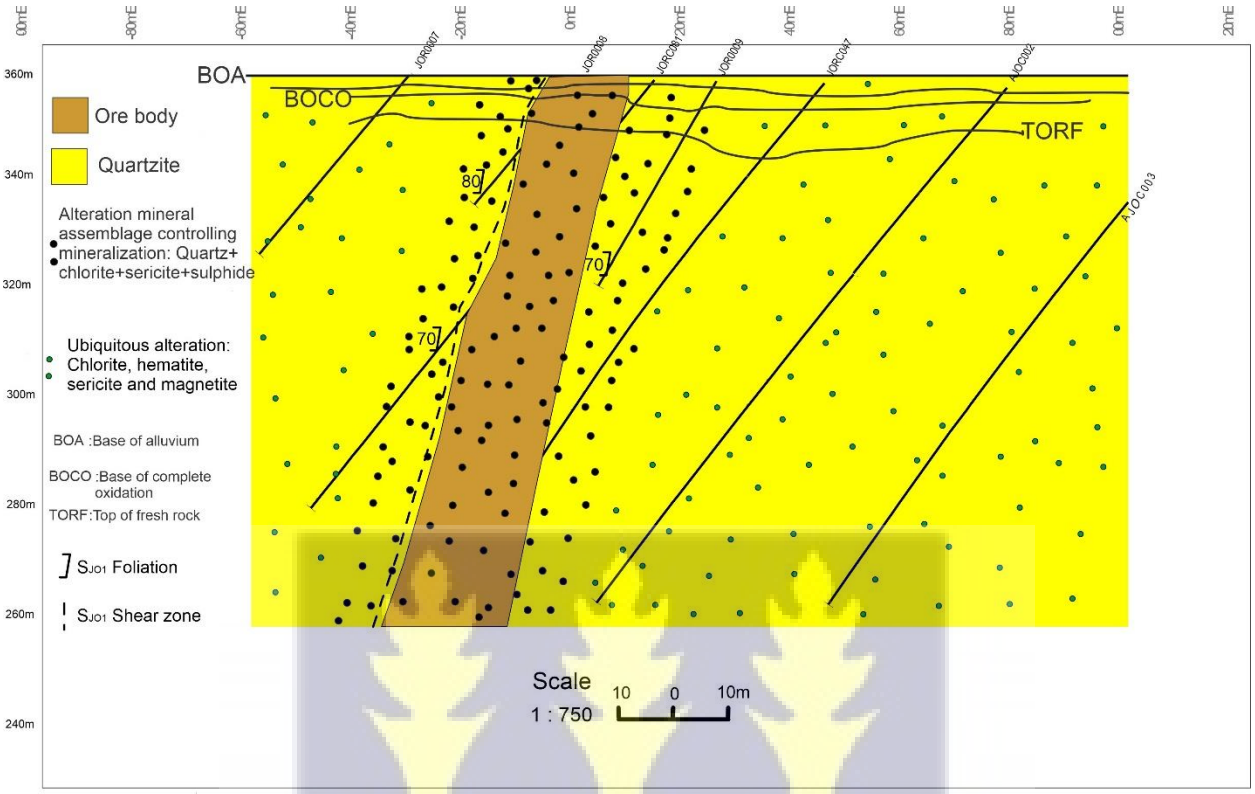

Figure 22. Cross-section (looking east) of the Josephine deposit along 576,450 mE showing the main ore body, along the NNW dextral D_{JO1} shear dipping 70-80° NE. High-grade mineralization is restricted to 15m to 40m thick alteration zone with alteration mineral assemblage of quartz+chlorite+sericite+sulphides.

4.4 Ore body characteristics and geometry

The main orebody in the Josephine deposit in general is associated with a steeper, NNW (clockwise) trending S_{JO1} shear zone within the generally NE-dipping sequence. This is interpreted as a right-stepping relay or sinusoidal shear bend. The mineralized zone is about 15m to 40m wide and 800m long. It occurs within a 20 to 120m thick alteration zone (Figure 22) above. Alteration mineral assemblage controlling the mineralization is quartz +chlorite + sericite+ sulphide while

alteration mineral assemblage of chlorite +hematite+ sericite+ magnetite appears to be ubiquitous across the whole study area.

Mineralization at Josephine deposit is not associated with strong veining. Minor stringers, grey quartz veins in drill core appear to pre-date main stage deformation and metamorphism.

4.5 Isocon Analysis (Mass-Balance considerations)

Grant (1986) developed the "Isocon" diagram as a simple solution to Gresens (1967) equation for analysing changes in volume and concentration in metasomatic alteration. This method was applied in the study of hydrothermal changes. It is possible to achieve this graphically by plotting an altered composition against an original composition with no significant data manipulation. The "Isocon", which is a straight line through the origin, is defined by species that have remained immobile during the process.

Quantitative evaluation of chemical gains and losses in the mineralized rocks (the quartzites) throughout the hydrothermal process has been estimated utilizing major-oxide and trace-element compositions determined by whole-rock geochemical analysis to further define the alteration (Table 2). To assess substantial changes in composition, mass, and volume, the Gresens-Grant (Grant, 1986, 2005; Gresens, 1967) isocon approach was utilized (Figure 23). Using the EASYGRESGRANT MS-Excel sheet given by Lopez-Moro (2012), modified in 2021 and applying the approach therein, average compositions for the least altered zones were plotted against average samples from the altered zones. Immobile elements were used as the reference frame for the analysis. The elements, zirconium, dysprosium, and holmium were used. The element zirconium (Zr) and Hafnium (Hf) was chosen because it is unlikely to be mobile in this

environment, while the REEs (Dysprosium, Dy and Holmium, Ho) are mainly immobile during hydrothermal alteration (Grant, 2005).

Table 2. Major and trace element analytical data of the mineralized quartzites in the Josephine deposit

	ALTERED SAMPLES					UNALTERED SAMPLES				
SAMPLE	JO01	JO03	JO04	JO08	JO06	JO02	JO07	JO09	JO10	JO05
wt%										
SiO_2	60.10	69.80	59.90	72.00	75.90	71.50	75.50	74.90	72.40	77.90
Al_2O_3	16.35	15.45	16.20	13.20	12.65	13.95	10.70	11.95	15.30	10.55
Fe_2O_3	6.92	4.93	6.22	6.01	3.44	4.81	6.39	5.18	2.55	4.37
CaO	4.19	1.97	5.11	1.77	2.84	2.10	1.87	1.54	2.03	1.48
MgO	3.22	1.51	2.75	1.87	0.41	1.55	0.35	1.09	0.55	0.51
Na_2O	4.22	3.43	4.48	3.43	3.31	2.52	4.69	4.48	4.94	4.92
K_2O	2.81	2.75	2.16	2.08	1.74	2.61	0.99	1.44	2.65	0.54
Cr_2O_3	0.07	0.06	0.03	0.07	0.09	0.07	0.08	0.08	0.07	0.08
TiO_2	0.72	0.65	0.75	0.60	0.28	0.57	0.49	0.32	0.44	0.22
MnO	0.09	0.09	0.09	0.04	0.05	0.08	0.11	0.10	0.02	0.07
P_2O_5	0.29	0.12	0.31	0.12	0.08	0.07	0.06	0.07	0.14	0.03
SrO	0.09	0.06	0.10	0.04	0.06	0.05	0.01	0.01	0.10	0.02
BaO	0.09	0.10	0.10	0.06	0.07	0.08	0.03	0.05	0.14	0.03
Total	**101.66**	**101.94**	**100.03**	**101.88**	**101.11**	**100.88**	**101.78**	**101.77**	**101.73**	**100.83**
ppm										
Ag	1.30	0.60	0.50	1.20	0.80	0.50	0.50	0.40	0.60	0.40
As	10.50	9.62	5.60	11.00	9.82	3.62	3.10	3.82	3.62	4.10
Au	2.20	0.82	4.10	3.40	0.86	0.06	0.04	0.05	0.02	0.05
Ba	774.00	890.00	820.00	525.00	563.00	695.00	259.00	457.00	1220.00	286.00
Cd	0.40	0.40	0.50	0.50	0.40	0.50	0.50	0.30	0.50	0.40
Ce	68.50	48.00	64.80	48.90	68.00	45.50	186.00	93.10	79.70	67.50
Co	11.00	10.50	16.00	12.00	11.00	14.00	15.50	15.00	14.00	12.00
Cr	480.00	460.00	170.00	480.00	670.00	500.00	600.00	550.00	520.00	620.00
Cs	3.58	5.82	3.94	3.66	4.11	9.67	0.73	2.74	2.19	0.47
Cu	26.00	23.00	28.00	38.00	26.00	10.00	9.50	8.00	9.50	11.00
Dy	2.75	2.69	2.72	2.51	1.79	2.34	21.40	16.45	1.00	14.45
Er	1.57	1.44	1.28	1.61	0.94	1.38	13.40	11.20	0.24	8.72
Eu	1.39	1.05	1.62	1.06	1.10	0.95	2.96	2.57	1.25	2.64
Ga	20.30	17.10	19.00	13.80	14.80	13.80	20.00	24.40	20.70	18.90
Gd	3.89	3.10	4.04	3.03	2.59	2.68	19.30	14.45	2.84	13.05
Hf	3.80	5.80	3.70	4.20	2.80	3.50	19.70	11.00	5.10	10.50
Ho	0.53	0.53	0.49	0.48	0.34	0.48	4.44	3.65	0.13	2.98
La	31.10	23.20	27.90	23.40	35.00	21.10	73.70	39.10	37.30	28.10
Li	0.50	0.60	0.50	0.52	0.50	12.00	15.00	18.00	11.00	15.00
Lu	0.22	0.24	0.19	0.22	0.15	0.20	1.98	1.77	0.03	1.15
Mo	0.60	2.20	3.40	0.50	3.40	3.60	4.10	3.20	3.10	0.80
Nb	4.90	5.40	4.30	4.50	4.10	4.80	31.20	18.40	3.90	14.00

Nd	34.60	20.90	32.10	20.60	25.00	19.70	85.20	52.60	34.30	42.80
Ni	28.00	26.00	36.00	34.00	16.00	34.00	36.00	18.00	16.00	22.00
Pb	6.80	6.40	14.00	16.00	11.00	11.00	10.50	11.00	12.00	9.50
Pr	8.74	5.45	8.13	5.57	7.17	5.27	21.40	12.40	9.30	9.55
Rb	79.20	72.20	49.70	64.80	52.90	75.40	20.40	51.20	58.10	4.20
S	0.22	0.25	0.28	0.30	0.23	0.08	0.06	0.12	0.08	0.09
Sb	8.24	6.22	18.20	16.50	3.00	0.05	0.11	0.08	0.12	0.12
Sc	11.00	10.50	12.00	10.00	10.50	12.00	11.00	10.50	9.00	9.50
Se	0.82	0.62	0.48	0.42	0.42	0.44	0.46	0.45	0.46	0.45
Sm	5.86	3.89	5.97	3.79	3.97	3.73	19.30	13.35	5.16	11.40
Sn	1.00	1.00	1.00	1.00	2.00	1.00	6.00	4.00	1.00	3.00
Sr	781.00	571.00	855.00	400.00	520.00	475.00	120.00	71.00	876.00	148.50
Ta	0.30	0.40	0.20	0.30	0.40	0.30	2.00	1.20	0.20	0.90
Tb	0.50	0.44	0.50	0.43	0.33	0.41	3.28	2.50	0.25	2.23
Te	6.20	6.20	6.50	7.10	6.60	0.04	0.05	0.05	0.02	0.02
Th	1.16	5.24	1.01	3.84	6.25	3.61	8.66	4.85	2.88	1.66
Tm	0.21	0.22	0.19	0.23	0.12	0.20	2.03	1.68	0.03	1.30
U	0.28	1.56	0.44	1.23	1.63	1.30	1.88	1.50	0.85	0.53
V	144.00	115.00	112.00	118.00	73.00	89.00	25.00	20.00	36.00	19.00
W	1.00	11.00	5.00	2.00	1.00	3.00	4.00	1.00	<1	<1
Y	14.70	14.80	13.40	13.60	9.40	12.10	119.00	99.50	3.80	80.40
Yb	1.45	1.48	1.25	1.47	0.87	1.31	12.90	11.05	0.16	7.98
Zr	146.00	224.00	157.00	164.00	101.00	132.00	825.00	440.00	199.00	427.00
Zn	62.00	55.71	65.00	57.60	65.00	69.10	72.00	77.20	71.20	75.00

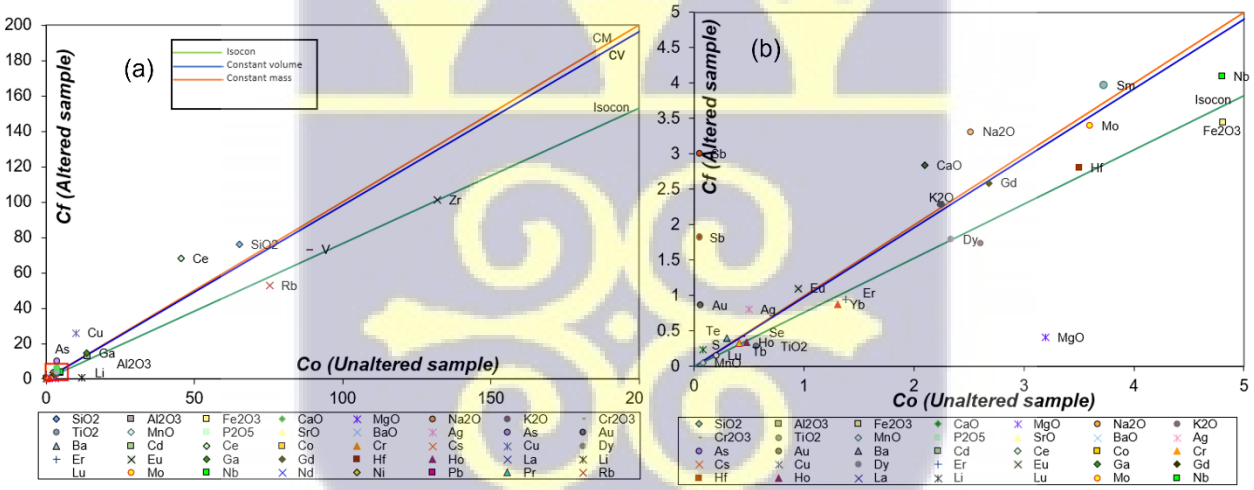

Figure 23. Isocon diagrams constructed (using the EASYGRESGRANT MS-Excel sheet in Lopez-Moro (2012); based on the theoretical development by Gresens', 1967 and built upon by Grant (1986)) for five pairs each of unaltered and altered quartzites from the main ore zone. (a) the Isocon diagram (b) shows a close-up of the red insert in (a)

The analysis revealed that, (Fig. 23) mass was largely retained during the alteration process. The elements gained in the process are Au, Te, S, Cu, Ag, Sm, Ce and Ta. For the major oxides, Al_2O_3 and MnO was constant in the system, SiO_2, Na_2O, K_2O and CaO were added to the system, and Fe_2O_3, TiO_2, were leached from the system. Table 3 below is a summary of the chemical gains and losses in the system.

Table 3. Whole-rock geochemical data from the alteration zone in the quartzites used for the isocon calculations.

Alteration (mineralized zone)				Least altered	
Number of samples	5		Gain/loss in wt% or ppm ΔCi/Co	5	
	Average (Ci_Ai)	1σ	Mass gain/loss	Average (Co)	1σ
	Mineralized			Unaltered	
Oxides (g/100g^{-1})					
SiO2	75.90	3.20	34.11	65.10	5.53
Al2O3	12.65	0.12	2.58	13.95	0.20
Fe2O3	3.44	0.01	-0.31	4.81	0.73
CaO	2.84	0.32	1.61	2.10	0.43
MgO	0.41	0.05	-2.66	3.20	1.13
Na2O	3.31	0.55	1.81	2.52	1.25
K2O	2.61	0.03	0.34	1.74	1.32
Cr2O3	0.09	0.01	0.05	0.07	0.01
TiO2	0.28	0.02	-0.20	0.57	0.27
MnO	0.05	0.01	-0.01	0.08	0.02
P2O5	0.08	0.04	0.03	0.07	0.03
SrO	0.06	0.03	0.03	0.05	0.02
BaO	0.07	0.01	0.01	0.08	0.02
Trace elements (100^{-3}g/100g^{-1})					
Ag	1.50	0.30	0.55	0.50	0.20
As	9.82	0.01	9.22	3.62	1.03
Au	3.50	0.01	1.06	0.06	0.01
Ba	563.00	16.00	40.90	695.00	54.00
Cd	0.40	0.03	0.02	0.50	0.31
Ce	68.00	4.20	43.38	45.50	7.34

Co	11.00	3.20	0.38	14.00	3.41
Cr	670.00	106.00	375.76	500.00	89.00
Cs	4.11	0.23	-4.30	9.67	1.62
Cu	26.00	2.00	23.98	10.00	3.00
Dy	1.79	0.12	0.00	2.34	0.24
Er	0.94	0.05	-0.15	1.38	0.51
Eu	1.10	0.11	0.49	0.95	0.07
Ga	14.80	2.20	5.55	13.80	3.54
Gd	2.59	1.10	0.71	2.68	1.07
Hf	2.80	0.24	0.16	3.50	1.71
Ho	0.34	0.10	-0.04	0.48	0.12
La	35.00	2.55	24.65	21.10	5.20
Li	0.50	0.00	-11.35	12.00	4.00
Lu	0.15	0.04	0.00	0.20	0.03
Mo	3.40	1.01	0.84	3.60	0.42
Nb	4.10	0.32	0.56	4.80	0.56
Nd	25.00	3.12	12.98	19.70	3.41
Ni	16.00	3.00	-13.09	34.00	6.00
Pb	11.00	2.12	3.38	11.00	2.00
Pr	7.17	1.43	4.10	5.27	0.91
Rb	52.90	5.53	-6.25	75.40	12.10
S	0.23	0.06	0.22	0.08	0.00
Sb	3.00	0.72	3.87	0.05	0.00
Sc	10.50	4.10	1.72	12.00	3.00
Se	0.42	0.08	0.11	0.44	0.04
Sm	3.97	1.30	1.46	3.73	0.14
Sn	2.00	0.63	1.61	1.00	0.00
Sr	520.00	115.70	204.69	475.00	27.00
Ta	0.40	0.01	0.22	0.30	0.04
Tb	0.33	0.00	0.02	0.41	0.02
Te	6.60	1.60	8.59	0.04	0.00
Th	6.25	0.54	4.56	3.61	0.50
Tm	0.12	0.03	-0.04	0.20	0.03
U	1.63	0.52	0.83	1.30	0.60
V	73.00	13.00	6.42	89.00	7.00
W	1.00	0.12	-1.69	3.00	1.00
Y	9.40	1.40	0.19	12.10	2.20
Yb	0.87	0.30	-0.17	1.31	0.42
Zr	101.00	9.34	0.02	132.00	29.00
Density g/cm3	3.77			3.74	

Ci_Ai = average concentration for alteration. Average of the unaltered samples segment in table 3 was used to define the least altered sample.

4.5 Ore Mineralogy

The textural analysis of sulphide minerals is key in providing important information and understandings into the origin, the history, and exploitability of the deposits, as well as potential problems in mineral processing. From petrographic analysis of sulphides, it is observed that disseminated arsenopyrite (Fig.24a), chalcopyrite and pyrite are the ore minerals (sulphides) recognized in the Josephine deposit. They occur along the foliations in the altered rocks and are associated with silicified zones. Arsenopyrite is the most dominant and frequently occurring sulphide. It is typically coarse grained, whitish in colour in SEM images, is euhedral and has a rhombic crystal shape. Arsenopyrite exhibits zoning. Chalcopyrite on the other hand grows on the arsenopyrite (Fig. 24c).

SEM image analysis together with field observation and petrographic analysis has revealed that the mineralization of gold in the Josephine deposit is associated with arsenopyrite occurrence. Gold is observed as disseminated inclusion in arsenopyrite (Fig.24b). It is observed in the SEM images that gold occurs with copper (Fig. 24d).

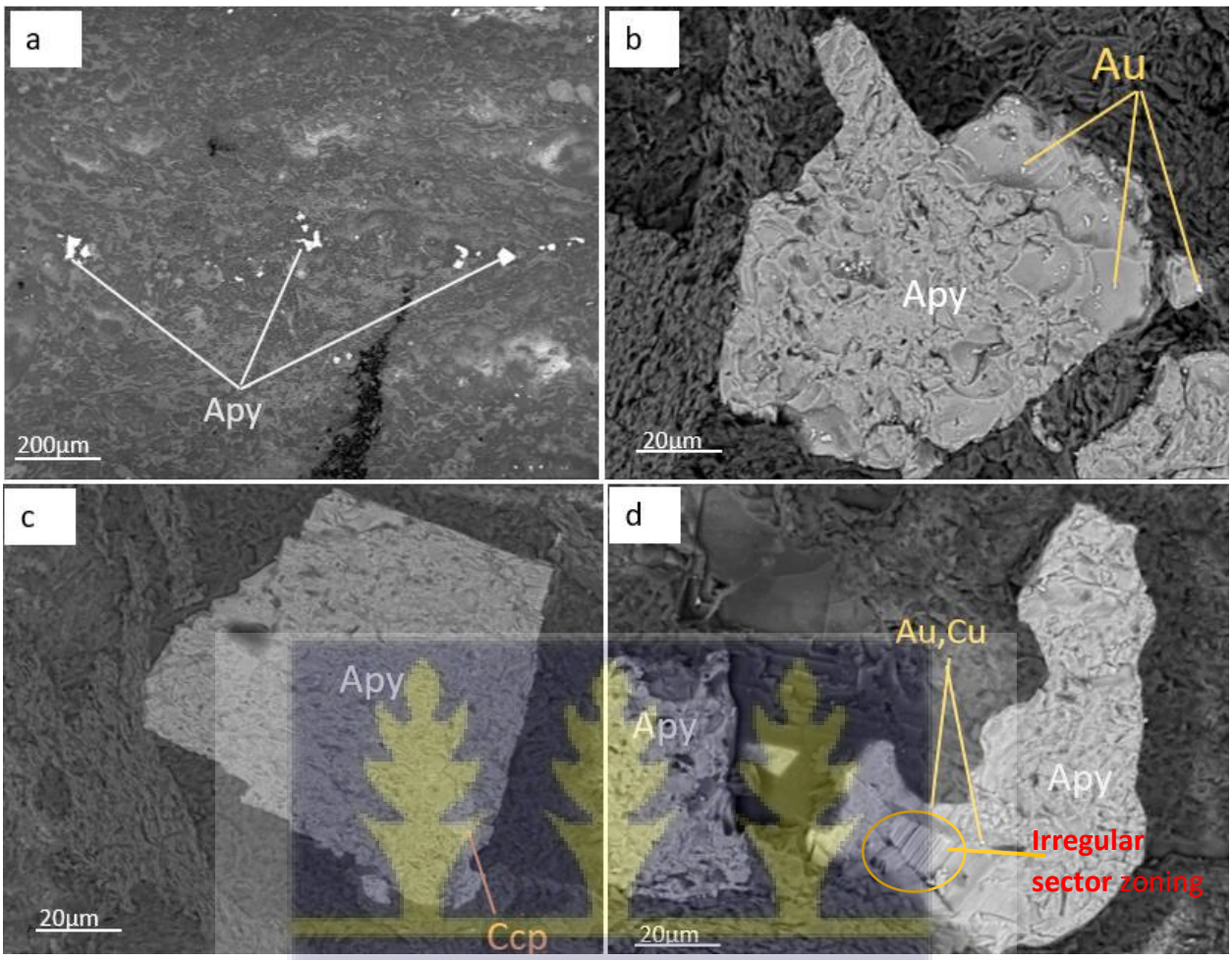

Figure 24. SEM images of arsenopyrites in the Josephine deposit (a) disseminated Arsenopyrite (b) gold occurrence in arsenopyrite (c) growth of chalcopyrite on arsenopyrite and (d) irregular sector zoning in arsenopyrite. Au=gold, Cu=copper, Apy=Arsenopyrite, Ccp=chalcopyrite.

CHAPTER FIVE

DISCUSSION

In this section, interpretation of the findings from field observation and laboratory analysis is made vis-à-vis known literature concerning the issue herein. Discussed here are; the lithology and metamorphism, the local structures in terms of the regional context and the structural and alteration controls on gold mineralization.

5.1 Lithology and Metamorphism

The petrographic analysis of rock samples from the field and drill data has shown that the rocks present in the study area includes granite, quartzite, dolerite and gneiss which is consistent with the works of Block et al. (2015) in the Bulenga domain and Amponsah et al., (2015) in the Julie belt. The quartzite is intruded by granite batholiths and dolerite (Fig.25).

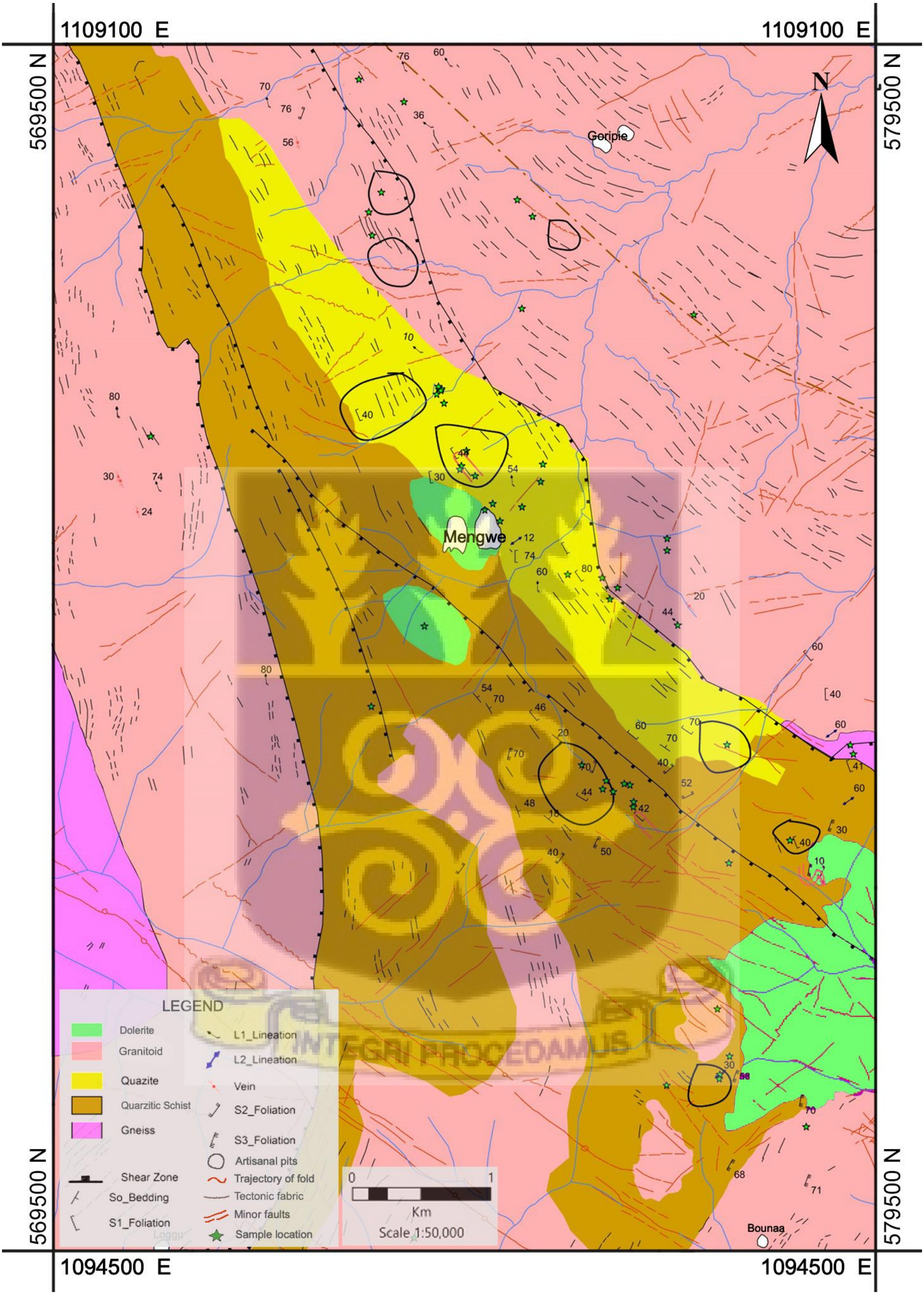

Figure 25. A simplified composite map of the Josephine deposit compiled from field data and geophysical data interpretation showing the lithological units, artisanal pits, and structures from both field measurement and geophysical data.

Metamorphism in the study area is mostly in the greenschist facies regime defined by quartz+chlorite+magnetite mineral assemblage with occurrence of micas in the quartzites, in accordance with the observation of Block et al. (2015), but for the south eastern portion of the study area where amphibolite facies marked by the occurrence of garnet is observed in the quartzites. The mineralized quartzites in the southern part of the study area has experienced retrograde metamorphism as some of the unmineralized quartzite has garnets as a major composition.

5.2 Situating the local structure into the regional structural context

Based on the structural analysis from both field mapping and drill cores, four localized deformational regimes have been identified in the Josephine deposit, herein named as D_{JO0}, D_{JO1}, D_{JO2} and D_{JO3}. The first phase of deformation is a shallow-to steeply dipping S_0 foliation, defined by preserved planar/tabular cross stratification with minerals exhibiting greenschist characteristics. This is mostly observed within the quartzite rock. D_{JO1} which in essence is the first episode of deformation whose occurrence is easily noticeable by a top-to-the-NE shallow- to steeply dipping S_{JO1} penetrative shear foliation (NW-SE trending) defined by an F_{JO1} fold (mostly isoclinal folds) and parallel to the stratigraphic layering (D_{JO0}). D_{JO1} correlates with the regional D_1 deformation event of initial NNE-SSW directed shortening, described by Baratoux et al., (2011) for the Birimian. The third deformation event (D_{JO2}) is defined by a NW-SE compression resulting into the formation of F_{JO2} folds (mostly open folds) with foliation generally dipping at an angle between 40°-70°. It correlates with the regional D_2 described by Baratoux et al., (2011). The final stage of deformation is the D_{JO3}. It is brittle-ductile deformation associated with an NNE-SSW S_{JO3} foliation (schistose cleavage), and dextral faulting. Folds in the form of ptygmatic folds and space cleavages, both of which formed as a result of a more E-W directed contraction is observed. This

deformational regime correlates with regional D_6 and D_3 deformation event as described by Block et al. (2015) for the Birimian of NW Ghana and Baratoux et al. (2011) for the Boromo belt respectively. The shear fabrics associated with the deformation in the Josephine deposit is indicative of pure shear/coaxial deformation. This means that the deformation is non-rigid and progressive (from D_{JO1}–D_{JO3}). The brittle-ductile nature of the deformation implies that the maximum depth and temperature of deformation is about 10–25 km and 500°C respectively.The table below summarizes the correlation between the local deformation events in the Josephine deposit and the regional events described by Block et al. (2015) and Baratoux et al. (2011).

Table 4. Table comparing the structures observed within the Josephine deposit and that of the regional deformation sequence proposed by Block (2015) and Baratoux et al., (2011)

Study	D_1	D_2	D_3	D_4	D_5	D_6
Block (2015) NW Ghana	D1= N-S directed shortening. E-W penetrative fabric (S1) with shallow to steep dips. Low angle thrust faulting and folding	D2= N-S directed shortening. S2 foliation with moderate dips with plunging lineation down dip	D3 =E-W directed shortening and S3 schistose foliation	D4=ENE to WSW shortening with sinistral strike slip shearing	D5= E-W brittle deformation	D6=E-W brittle deformation, tension and brittle strike and slip fault
Baratoux et al. (2011) Boromo belt			D1 = N-NNE oriented S1 foliation. F1 fold with axial pane parallel to S1	D2 consist of steeply dipping NNE to ENE anastomosing shear zone with dextral characteristics		D3 consist of crenulation cleavages, chevron kink folds, E-W space cleavages, and the late brittle strike slip faults
Josephine Deposit			D_{JO1}= NE-SW shortening. Consist of steeply dipping NE dextral sinusoidal shear bend with S_{JO1} shear foliation and F_{JO1} isoclinal fold	D_{JO2}=NE-SW trending S_{JO2} foliation defined by F_{JO2} open folds. Lineation plunges down-dip		D_{JO3}= E-W directed shortening. Brittle-ductile deformation and S_{JO3} schistose foliation axial planar to ptygmatic folds and E-W space cleavages.

5.1 structural and alteration controls on gold mineralization in the Josephine deposit.

5.1.1 Structural controls on mineralization

The mineralization in the Josephine deposit is directly related to the shallow-to-steeply dipping dextral shear foliation (D_{JO1} deformational event). In the ore zone, the shear zone has a shallow-to-steeply dipping (subvertical) S_{JO1} penetrative shear foliation indicating a footwall and a hanging wall. The hanging wall shows shallow dips and the foot wall shows steep dips in the mineralization zone. The fault plane is the zone of weakness and acts as the plumbing or fluid pathway for the gold mineral to precipitate within the complex.

Gold mineralization in the Josephine deposit is not associated with strong veining but well associated with the alteration (silicification bleaching), however, minor veinlets observed in the mineralization zone in rock outcrops and in drill cores are significantly mineralized. In general, the mineralized zone seems associated with a steeper more NNW trending zone within the generally NE-dipping sequence. This is interpreted as a right-stepping relay or sinusoidal shear bend as indicated by the shallow-to-steep dips in the mineralized zone. This is described as releasing bends or dilatational jogs by Groshong Jr (1988) and Sibson (1996) respectively. This is compatible with a dextral and thrust movement sense on the Josephine fault zone. The shear deformation which resulted into brittle-ductile faulting, permitted the plumbing of the mineralizing fluid, giving rise to the main dilatational structures and the resultant gold mineralization.

From the ongoing discussion, the structural history of gold mineralization documented in the Josephine deposit differs from that known in southern Ghana, described by (Allibone et al., 2004, Feybesse et al., 2006), that gold mineralization is primarily associated with late, brittle–ductile reactivation of faults with an early history of reverse movement with sinistral characteristics, compatible with the structural timing of a single mineralizing event. Gold mineralization in the

Josephine deposit is associated with a more early shear dextral and ductile shear zone with reverse movement similar to the Julie deposit described by (Amponsah et al., 2015).

5.1.2 Alteration controls on mineralization

The quartzites in the mineralized zone have been significantly altered, with alteration mineral assemblage of quartz, chlorite, sericite, arsenopyrite, and occasionally pyrite or chalcopyrite, or a combination of all. Chlorite and magnetite are ubiquitous in the study area, but chlorite in the mineralized zone is extremely intense.

In the alteration zone, sulphides largely replace magnetite. This kind of alteration mineralogy is consistent with the region's greenschist metamorphic grade. The isocon diagrams (Fig.23) shows the geochemical variations associated with the alteration. From the isocon graph, it is observed that the alteration was accompanied by a volume increase of approximately 16.59%. The alteration was accompanied by Au, Te, S, Cu, Ag, Sb, and Ta additions, as well as variations in Ca, Si, K, Na, Fe, and Ti, which are mostly consistent with the sulfidation, sericitization, silicification, and chloritization that affected the host rock. The presence of additional silica in the mineralized zone was anticipated, as it reflects the addition of quartz in the rock. The leaching of Fe in the mineralized zone was most likely caused by the extensive replacement of magnetite by arsenopyrite. The addition of K in system is as a result of the presence of sericite; an altered form of feldspars and micas. Furthermore, the Au–Sb association seen in the isocon graph is typical of orogenic Au deposits with depth of formation and temperature akin to a shallow crustal levels and relatively low temperatures (Groves et al., 1998). The significant width of the alteration zone implies that the fluid circulated throughout the entire shear corridor.

It was also observed from the field observation, petrographic work, and SEM imagery of mineralized quartzites, that gold mineralization in the Josephine is associated with arsenopyrite

formation. The presence of gold in arsenopyrite indicates that it was incorporated in solid solution during the precipitation of arsenopyrite. This kind of relationship between gold and arsenopyrite has been documented in numerous deposits around the world e.g., (Dalstra et al., 1997; Fougerouse et al., 2016; Genkin et al., 1998; Morey et al., 2008; Neumayr et al., 1993; Sung et al., 2009; Tarnocai et al., 1997; Tomkins & Mavrogenes, 2001; Yang & Zhou, 2001)

Gold in the Josephine has been identified as inclusions and free gold in arsenopyrite or occurs very close to it. The small gold inclusions in arsenopyrite are most likely the result of gold co-precipitation with the sulphide (Reich et al., 2005; Simon et al., 1999).

The SEM images also shows that most of the arsenopyrites in the Josephine deposits display evidence of As-S compositional zoning in the form of irregular sector zoning. The zoning and alteration in the sulphides indicates that they were formed during hydrothermal alteration processes.

CHAPTER SIX

CONCLUSION

Ensuing from the above discussion on the field observation, petrographic analysis, structural analysis and isocon analysis, the following conclusion can be made on the Josephine deposit;

1. The gold mineralization within the Josephine deposit is mainly associated with D_{JO1} deformational regime which is a steeply dipping dextral (right-stepping) relay or sinusoidal shear bend.
2. Gold occurs mostly as inclusions in the arsenopyrite mineral along S_{JO1} foliation or as free gold in the fractures.
3. Alteration assemblage directly associated with the mineralization zone in Josephine is quartz + chlorite + sericite+ sulphide assemblages.

RECOMMENDATION

The following recommendations will greatly improve upon our understaning of the structural and alteration controls of gold mineralization in the Josephine deposit:

1. Fluid inclusion study: The study of fluid inclusions reveals geologically significant information such as temperature, pressure, salinity, density, and trapping depth; providing direct information about the conditions under which given minerals and rocks form. This study can help improve our understanding of the conditions under which the gold was formed.
2. Whole-rock geochemistry for all the rock types in the study area to support the petrographic data and for petrogenesis studies in classification of the rocks.

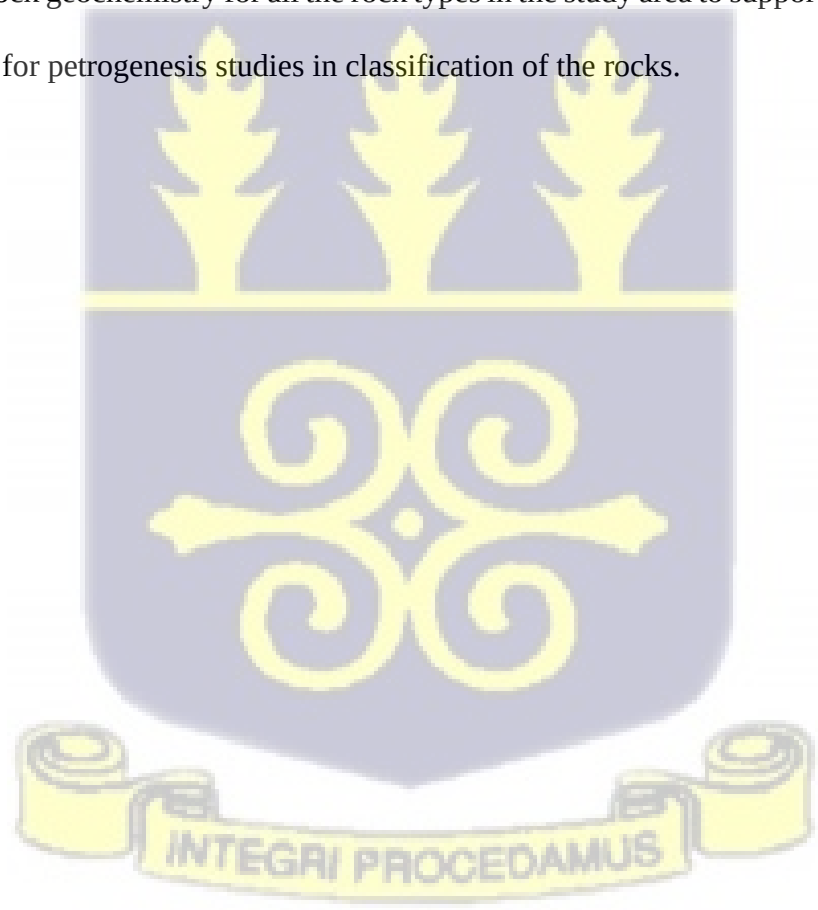

REFERENCES

Abouchami, W., Boher, M., Michard, A., & Albarede, F. (1990). A major 2.1 Ga event of mafic magmatism in West Africa: an early stage of crustal accretion. *Journal of Geophysical Research: Solid Earth*, *95*(B11), 17605-17629.

Adadey, K., Clarke, B., Théveniaut, H., Urien, P., Delor, C., Roig, J., & Feybesse, J. (2009). Geological map explanation-Map sheet 0503 B (1: 100 000), CGS/BRGM/Geoman. *Geological Survey Department of Ghana (GSD)*.

Allibone, A., Hayden, P., Cameron, G., & Duku, F. (2004). Paleoproterozoic gold deposits hosted by albite-and carbonate-altered tonalite in the Chirano District, Ghana, West Africa. *Economic Geology*, *99*(3), 479-497.

Allibone, A., Teasdale, J., Cameron, G., Etheridge, M., Uttley, P., Soboh, A., Appiah-Kubi, J., Adanu, A., Arthur, R., & Mamphey, J. (2002). Timing and structural controls on gold mineralization at the Bogoso gold mine, Ghana, West Africa. *Economic Geology*, *97*(5), 949-969.

Amponsah, P. O., Salvi, S., Béziat, D., Baratoux, L., Siebenaller, L., Nude, P. M., Nyarko, R. S., & Jessell, M. W. (2016). The Bepkong gold deposit, northwestern Ghana. *Ore Geology Reviews*, *78*, 718-723.

Amponsah, P. O., Salvi, S., Béziat, D., Siebenaller, L., Baratoux, L., & Jessell, M. W. (2015). Geology and geochemistry of the shear-hosted Julie gold deposit, NW Ghana. *Journal of African Earth Sciences*, *112*, 505-523.

Baratoux, L., Metelka, V., Naba, S., Jessell, M. W., Grégoire, M., & Ganne, J. (2011). Juvenile Paleoproterozoic crust evolution during the Eburnean orogeny (~ 2.2–2.0 Ga), western Burkina Faso. *Precambrian Research*, *191*(1-2), 18-45.

Block, S., Ganne, J., Baratoux, L., Zeh, A., Parra-Avila, L., Jessell, M., Ailleres, L., & Siebenaller, L. (2015). Petrological and geochronological constraints on lower crust exhumation during Paleoproterozoic (Eburnean) orogeny, NW Ghana, West African Craton. *Journal of Metamorphic Geology*, *33*(5), 463-494.

Block, S., Jessell, M., Aillères, L., Baratoux, L., Bruguier, O., Zeh, A., Bosch, D., Caby, R., & Mensah, E. (2016). Lower crust exhumation during Paleoproterozoic (Eburnean) orogeny, NW Ghana, West African Craton: interplay of coeval contractional deformation and extensional gravitational collapse. *Precambrian Research*, *274*, 82-109.

Boher, M., Abouchami, W., Michard, A., Albarede, F., & Arndt, N. T. (1992). Crustal growth in west Africa at 2.1 Ga. *Journal of Geophysical Research: Solid Earth*, *97*(B1), 345-369.

Dalstra, H., Bloem, E., Ridley, J., & Groves, D. (1997). Diapirism synchronous with regional deformation and gold mineralisation, a new concept for granitoid emplacement in the Southern Cross Province, Western Australia. *Geologie en Mijnbouw*, *76*(4), 321-338.

Davis, D., Hirdes, W., Schaltegger, U., & Nunoo, E. (1994). U□ Pb age constraints on deposition and provenance of Birimian and gold-bearing Tarkwaian sediments in Ghana, West Africa. *Precambrian Research*, *67*(1-2), 89-107.

De Kock, G., Armstrong, R., Siegfried, H., & Thomas, E. (2011). Geochronology of the Birim Supergroup of the West African craton in the Wa-Bolé region of west-central Ghana: Implications for the stratigraphic framework. *Journal of African Earth Sciences*, *59*(1), 1-40.

Dickson, K. B., & Benneh, G. (1988). *A Geography of Ghana*. London: Longman.

Doumbia, S., Pouclet, A., Kouamelan, A., Peucat, J., Vidal, M., & Delor, C. (1998). Petrogenesis of juvenile-type Birimian (Paleoproterozoic) granitoids in Central Côte-d'Ivoire, West Africa: geochemistry and geochronology. *Precambrian Research, 87*(1-2), 33-63.

Duodu, J. A. (2009). *Geological Map of Ghana 1: 1 000 000*. Geological Survey Department.

Eisenlohr, B., & Hirdes, W. (1992). The structural development of the early Proterozoic Birimian and Tarkwaian rocks of southwest Ghana, West Africa. *Journal of African Earth Sciences (and the Middle East), 14*(3), 313-325.

Feybesse, J.-L., Billa, M., Guerrot, C., Duguey, E., Lescuyer, J.-L., Milesi, J.-P., & Bouchot, V. (2006). The paleoproterozoic Ghanaian province: geodynamic model and ore controls, including regional stress modeling. *Precambrian Research, 149*(3-4), 149-196.

Feybesse, J.-L., & Milési, J.-P. (1994). The Archaean/Proterozoic contact zone in West Africa: a mountain belt of décollement thrusting and folding on a continental margin related to 2.1 Ga convergence of Archaean cratons? *Precambrian Research, 69*(1-4), 199-227.

Fossen, H. (2016). *Structural geology*. Cambridge university press.

Fougerouse, D., Micklethwaite, S., Tomkins, A. G., Mei, Y., Kilburn, M., Guagliardo, P., Fisher, L. A., Halfpenny, A., Gee, M., & Paterson, D. (2016). Gold remobilisation and formation of high grade ore shoots driven by dissolution-reprecipitation replacement and Ni substitution into auriferous arsenopyrite. *Geochimica et Cosmochimica acta, 178*, 143-159.

Fougerouse, D., Micklethwaite, S., Ulrich, S., Miller, J., Godel, B., Adams, D. T., & McCuaig, T. C. (2017). Evidence for two stages of mineralization in West Africa's largest gold deposit: Obuasi, Ghana. *Economic Geology, 112*(1), 3-22.

Further Africa. (2020). *Ghana still Africa's largest gold producer in 2021 – Fitch*. https://furtherafrica.com/2020/11/10/ghana-still-africas-largest-gold-producer-in-2021-fitch/

Genkin, A. D., Bortnikov, N. S., Cabri, L. J., Wagner, F., Stanley, C. J., Safonov, Y. G., McMahon, G., Friedl, J., Kerzin, A. L., & Gamyanin, G. N. (1998). A multidisciplinary study of invisible gold in arsenopyrite from four mesothermal gold deposits in Siberia, Russian Federation. *Economic Geology*, *93*(4), 463-487.

Government of Ghana. (2020a). *Upper West Region, Soil*. https://www.mofa.gov.gh/site/directorates/regional-directorates/upper-west-region

Government of Ghana. (2020b). *Upper West Region, Vegetation* https://www.mofa.gov.gh/site/directorates/regional-directorates/upper-west-region

Grant, J. A. (1986). The isocon diagram; a simple solution to Gresens' equation for metasomatic alteration. *Economic Geology*, *81*(8), 1976-1982.

Grant, J. A. (2005). Isocon analysis: A brief review of the method and applications. *Physics and Chemistry of the Earth, Parts A/B/C*, *30*(17-18), 997-1004.

Gresens, R. L. (1967). Composition-volume relationships of metasomatism. *Chemical geology*, *2*, 47-65.

Groshong Jr, R. H. (1988). Low-temperature deformation mechanisms and their interpretation. *Geological Society of America Bulletin*, *100*(9), 1329-1360.

Groves, D. I., Goldfarb, R. J., Gebre-Mariam, M., Hagemann, S. G., & Robert, F. (1998). Orogenic gold deposits: a proposed classification in the context of their crustal distribution and relationship to other gold deposit types. *Ore Geology Reviews*, *13*(1-5), 7-27.

Hirdes, W., Davis, D., & Eisenlohr, B. (1992). Reassessment of Proterozoic granitoid ages in Ghana on the basis of U/Pb zircon and monazite dating. *Precambrian Research*, *56*(1-2), 89-96.

Ibaera Capital. (2021). *Key Metrics*. https://ibaera.com/project-news/black-volta-gold-project-ghana/

International trade organization. (2020). *Mining Industry*. https://www.trade.gov/country-commercial-guides/ghana-mining-industry-equipment#:~:text=Gold%20is%20the%20most%20commercially,South%20Africa's%204.2%20million%20ounces.

Jin, L., Whitehead, P. G., Addo, K. A., Amisigo, B., Macadam, I., Janes, T., Crossman, J., Nicholls, R. J., McCartney, M., & Rodda, H. J. (2018). Modeling future flows of the Volta River system: Impacts of climate change and socio-economic changes. *Science of the Total Environment*, *637*, 1069-1080.

Junner, N. (1940). Geology of the gold coat and Western Togoland. *Bull. Gold Coast Geol. Surv.*, *11*, 40.

Junner, N. R., & Wild, R. (1935). *Gold in the gold coast*. Government Printer.

Kitson, A. (1918). Annual Report for 1916/17. *Gold Coast Geological Survey*.

Ledru, P., Johan, V., Milési, J. P., & Tegyey, M. (1994). Markers of the last stages of the Palaeoproterozoic collision: evidence for a 2 Ga continent involving circum-South Atlantic provinces. *Precambrian Research*, *69*(1-4), 169-191.

Ledru, P., Milési, J., Vinchon, C., Ankrah, P., Johan, V., & Marcoux, E. (1988). Geology of the Birimian series of Ghana. International Conference and Workshop on the Geology of Ghana with Special Emphasis on Gold Programme and Abstracts, Accra, Ghana,

Lopez-Moro, F. J. (2012). EASYGRESGRANT—A Microsoft Excel spreadsheet to quantify volume changes and to perform mass-balance modeling in metasomatic systems. *Computers and Geosciences*, *39*, 191.

Macrotrends. (2021). *Gold Prices*. https://www.macrotrends.net/1333/historical-gold-prices-100-year-chart

McCartney, M., Forkuor, G., Sood, A., Amisigo, B., Hattermann, F., & Muthuwatta, L. (2012). *The water resource implications of changing climate in the Volta River Basin* (Vol. 146). IWMI.

Milési, J.-P., Ledru, P., Feybesse, J.-L., Dommanget, A., & Marcoux, E. (1992). Early Proterozoic ore deposits and tectonics of the Birimian orogenic belt, West Africa. *Precambrian Research*, *58*(1-4), 305-344.

Morey, A. A., Tomkins, A. G., Bierlein, F. P., Weinberg, R. F., & Davidson, G. J. (2008). Bimodal distribution of gold in pyrite and arsenopyrite: Examples from the Archean Boorara and Bardoc shear systems, Yilgarn craton, Western Australia. *Economic Geology*, *103*(3), 599-614.

Neumayr, P., Cabri, L., Groves, D., Mikucki, E., & Jackman, J. A. (1993). The mineralogical distribution of gold and relative timing of gold mineralization in two Archean settings of high metamorphic grade in Australia. *The Canadian Mineralogist*, *31*(3), 711-725.

Oberthür, T., Vetter, U., Davis, D. W., & Amanor, J. A. (1998). Age constraints on gold mineralization and Paleoproterozoic crustal evolution in the Ashanti belt of southern Ghana. *Precambrian Research*, *89*(3-4), 129-143.

Perrouty, S., Aillères, L., Jessell, M. W., Baratoux, L., Bourassa, Y., & Crawford, B. (2012). Revised Eburnean geodynamic evolution of the gold-rich southern Ashanti Belt, Ghana,

with new field and geophysical evidence of pre-Tarkwaian deformations. *Precambrian Research*, *204*, 12-39.

Petr, T. (1986). The Volta river system. In *The ecology of river systems* (pp. 163-199). Springer.

Pigois, J.-P., Groves, D. I., Fletcher, I. R., McNaughton, N. J., & Snee, L. W. (2003). Age constraints on Tarkwaian palaeoplacer and lode-gold formation in the Tarkwa-Damang district, SW Ghana. *Mineralium Deposita*, *38*(6), 695-714.

Pouclet, A., Doumbia, S., & Vidal, M. (2006). Geodynamic setting of the Birimian volcanism in central Ivory Coast (western Africa) and its place in the Palaeoproterozoic evolution of the Man Shield. *Bulletin de la Société Géologique de France*, *177*(2), 105-121.

Reich, M., Kesler, S. E., Utsunomiya, S., Palenik, C. S., Chryssoulis, S. L., & Ewing, R. C. (2005). Solubility of gold in arsenian pyrite. *Geochimica et Cosmochimica acta*, *69*(11), 2781-2796.

Sakyi, P. A., Su, B.-X., Anum, S., Kwayisi, D., Dampare, S. B., Anani, C. Y., & Nude, P. M. (2014). New zircon U–Pb ages for erratic emplacement of 2213–2130 Ma Paleoproterozoic calc-alkaline I-type granitoid rocks in the Lawra Volcanic Belt of Northwestern Ghana, West Africa. *Precambrian Research*, *254*, 149-168.

Salvi, S., Amponsah, P. O., Siebenaller, L., Béziat, D., Baratoux, L., & Jessell, M. (2016). Shear-related gold mineralization in Northwest Ghana: The Julie deposit. *Ore Geology Reviews*, *78*, 712-717.

Sibson, R. H. (1996). Structural permeability of fluid-driven fault-fracture meshes. *Journal of Structural Geology*, *18*(8), 1031-1042.

Simon, G., Huang, H., Penner-Hahn, J. E., Kesler, S. E., & Kao, L.-S. (1999). Oxidation state of gold and arsenic in gold-bearing arsenian pyrite. *American Mineralogist*, *84*(7-8), 1071-1079.

Sung, Y.-H., Brugger, J., Ciobanu, C., Pring, A., Skinner, W., & Nugus, M. (2009). Invisible gold in arsenian pyrite and arsenopyrite from a multistage Archaean gold deposit: Sunrise Dam, Eastern Goldfields Province, Western Australia. *Mineralium Deposita*, *44*(7), 765-791.

Tarnocai, C. A., Hattori, K., & Cabri, L. J. (1997). " Invisible" gold in sulfides from Campbell Mine, Red lake greenstone belt, Ontario; evidence for mineralization during the peak of metamorphism. *The Canadian Mineralogist*, *35*(4), 805-815.

Taylor, W. R., Tompkins, L. A., & Haggerty, S. E. (1994). Comparative geochemistry of West African kimberlites: evidence for a micaceous kimberlite endmember of sublithospheric origin. *Geochimica et Cosmochimica acta*, *58*(19), 4017-4037.

Terry, R. D., & Chilingar, G. V. (1955). Summary of" Concerning some additional aids in studying sedimentary formations," by MS Shvetsov. *Journal of Sedimentary Research*, *25*(3), 229-234.

Tomkins, A. G., & Mavrogenes, J. A. (2001). Redistribution of gold within arsenopyrite and lollingite during pro-and retrograde metamorphism: Application to timing of mineralization. *Economic Geology*, *96*(3), 525-534.

Vidal, M., Gumiaux, C., Cagnard, F., Pouclet, A., Ouattara, G., & Pichon, M. (2009). Evolution of a Paleoproterozoic “weak type” orogeny in the West African Craton (Ivory Coast). *Tectonophysics*, *477*(3-4), 145-159.

Whitelaw, O. A. L., & Junner, N. R. (1929). *The geological and mining features of the Tarkwa-Abosso Goldfield*. Geological Survey.

Yang, J.-H., & Zhou, X.-H. (2001). Rb-Sr, Sm-Nd, and Pb isotope systematics of pyrite: Implications for the age and genesis of lode gold deposits. *Geology, 29*(8), 711-714.

Appendix 1: Attitude of Bedding plane

Dip Direction	Dip
120	40
46	20
38	20
38	18
102	50
88	60
94	50
70	48
50	54
60	70
34	70
44	48
52	50
40	22
38	26
54	30

Appendix 2: Attitude of foliation (S_{JO1})

Dip Direction	Dip
070	41
030	67
060	40
030	40
060	88
080	60
068	40
080	40
098	80
050	60
088	40
030	60
018	70
050	42
044	42
038	60
060	62
034	18
036	70
086	20
068	20
070	40
046	20
038	20
038	18
090	74
070	48
050	54
060	70
034	70
068	60
060	42
082	30
056	80
060	12

Appendix 3: Attitude of foliation (S_{JO2})

Dip Direction	Dip
350	10
308	40
318	40
342	38
338	40
340	50
340	45
335	52
250	58
260	70
306	30
256	70
240	80
260	76
320	42
316	52
330	44
308	32
294	50
310	40
342	50

Appendix 4: Attitude of foliation (S_{JO3})

Dip Direction	Dip
104	70
110	58
116	50
110	48
140	72
110	70
110	30
119	25
140	71
138	70
140	68
120	50
130	60
140	30
122	64
134	46
136	48

Appendix 5: Attitude of lineation (L_{JO1})

Trend	Plunge
060	38
040	40
082	41
040	60
040	60
090	12
020	70
032	30
022	20
032	32
052	32
050	34
030	26
040	28
044	30
	38
	40

Appendix 6: Attitude of lineation (L_{JO2})

Trend	Plunge
310	10
238	50
340	42
350	50
304	36
358	60
360	58
360	56
358	58
326	20
320	50
328	30
324	80
320	80
336	72
360	60
354	54
360	80
350	86
354	80
350	80
340	74
356	80
310	44
350	70
348	70
344	76
328	60